Stability Properties of High-Beta Geotail Flux Tubes

W. Horton, H.V. Wong, J.W. Van Dam, and C. Crabtree

Institute for Fusion Studies, The University of Texas at Austin, Austin, Texas 78712

Abstract

Kinetic theory is used to investigate the stability of ballooning-interchange modes in the high pressure geotail plasma. A variational form of the stability problem is used to compare new kinetic stability results with MHD, Fast-MHD, and Kruskal-Oberman stability results. Two types of drift modes are analyzed. A kinetic ion pressure gradient drift wave with a frequency given by the ion diamagnetic drift frequency ω_{*pi}, and a very low-frequency mode $|\omega| \ll \omega_{*pi}, \omega_{Di}$ that is often called a convective cell or the trapped particle mode. In the high-pressure geotail plasma a general procedure for solving the stability problem in a $1/\beta$ expansion for the minimizing $\delta B_{\|}$ is carried out to derive an integral-differential equation for the kinetically valid displacement field ξ^{ψ} for a flux tube. The plasma energy released by these modes is estimated in the nonlinear state. The role of these instabilities in substorm dynamics is assessed in the substorm scenarios described in Maynard *et al.* (1996).

Keywords: 2736 Magnetospheric physics; Magnetosphere/ionosphere interactions 2744; Magnetotail 2752; MHD waves and instabilities 2788; Storms and substorms

I. INTRODUCTION

A key component of quantitative modeling of magnetic substorms is to understand the stability of the stretched nightside geomagnetic flux tubes. The plasma is a hot ion plasma with a ratio $\beta = 2\mu_0 p/B^2$ of plasma pressure to magnetic pressure that varies strongly with position, reaching values greater than unity at the equatorial plane. The plasma pressure is confined by magnetic field loops whose curvature vector $\boldsymbol{\kappa} = (\boldsymbol{b}\cdot\nabla)\boldsymbol{b}$ is strongly peaked at the equatorial plane, where the Earthward pressure gradient dp/dx is also a maximum. Under conditions whose details are still strongly debated in the literature, the product of the pressure gradient and the curvature can allow a spontaneous local interchange of flux tubes that lower the energy of the system such that $\delta W < 0$. In such regions, an initial disturbance $\boldsymbol{\xi}$ with a strong East-West variation described by wavenumbers $k_y \gg k_x \gg k_\parallel$ grows exponentially at the rate of the fast MHD interchange growth rate $\gamma_{\rm mhd} = (dp/\rho R_c dx)^{1/2} = v_i/(L_p R_c)^{1/2}$. Here L_p is the pressure gradient scale length and R_c^{-1} is the (equitorial) value of $\max|\boldsymbol{\kappa}|$, and $v_i = (T_i/m_i)^{1/2}$ is the ion thermal velocity. The coordinates are the GSM orthogonal x, y, z coordinates, which are centered on the Earth with $\widehat{\boldsymbol{x}}$ directed toward the sun, $\widehat{\boldsymbol{y}}$ in the Earth's elliptic plane, and $\widehat{\boldsymbol{z}}$ in the northward direction in the plane defined by the Earth's magnetic dipole axis and $\widehat{\boldsymbol{x}}$. The GSM coordinates are appropriate for geotail physics where the solar wind controls the direction of currents and pressure gradients rather than the near-Earth dipole field. There are two immediately apparent conditions for the growth to occur: viz., the interchange energy released must exceed both (i) the energy involved in compressing the plasma $\delta W_{\rm comp} \propto pV(\kappa\xi_r)^2 > 0$ where ξ_r is the tailward displacement of the flux tube, and also (ii) the energy increase that results from disturbing and bending the magnetic field lines, given by the flux tube integrals of $\delta B_\parallel^2/2\mu_0$ and $\delta B_\perp^2/2\mu_0$, respectively. Here $V = \int ds/B$ is the volume of the flux tube. In Horton *et al.* (1999), the result of the stability analysis is that the range of β between β_1 and β_2 is unstable with β_1 set by line bending stabilization and β_2 by the compressional energy. The result is shown schematically in Fig. 1. Fig1

These precise stability conditions derived from the constraints are complex and depend greatly on the dynamical description of the plasma. For fast modes ($|\omega| > \omega_{*pi}, \omega_{Di}, \omega_{bi}$), the MHD description is adequate, and the results of Lee and Wolf (1992) and Lee (1998, 1999) and others apply and are reviewed in Sec. IV. Typically the growth rate computed from the MHD theory is not sufficiently fast to justify the MHD description, particularly at realistic values of k_x, k_y and $k_\parallel$. Some recent works by Sundaram and Fairfield (1997), Cheng and Lui (1998), and Horton *et al.* (1999) emphasize this point, viz., that a kinetic description of the geotail stability problem is required for substorm stability theory.

There is considerable observational evidence to suggest that in the early stage of substorm development there are westward propagating magnetic oscillations on auroral field lines (Roux *et al.*, 1991, Maynard *et al.*, 1996) in the transitional range between the dipole-dominated potential-like field region ($\boldsymbol{B}_{dp} = -\nabla\Phi_{dp}$) and the high beta geotail plasma field region in which $\mu_0 j_y \cong \partial B_x/\partial z \gg \partial B_z/\partial x$. The details of the transitional formulas are given in the Appendix. Figure 2 shows the transitional profiles of B_z, p, j_y and β computed from the Tsyganenko 96 equilibrium, compared with a local 2D equilibrium model used in analytic stability calculations. Since the stability of the flux tube depends on the equilibrium gradients in its neighborhood, the model with $j_y = dp/d\psi = \text{const}$ and a vacuum dipole field is generally adequate. Fig2

Horton *et al.* (1999) concluded that fast-growing interchange-ballooning fluctuations that satisfy the validity conditions for the hydrodynamic modes arise only in this transitional region. Although Lee (1999) reported finding marginally MHD conditions throughout the geotail (with the condition of $\boldsymbol{B}\cdot\nabla(\nabla\cdot\boldsymbol{\xi}) = 0$ imposed), the values of the growth rate from the $\delta W^{\rm MHD} < 0$ calculation are too slow (growth time $> 100\,$s) to be valid within the MHD model. Thus, we essentially disagree with his conclusion that the geotail is MHD unstable for $\beta > \beta_2 \gg 1$.

In contrast with Fig. 4 in Lee (1999) that shows $\delta W^{\rm MHD}$ (Fast)> 0 for the fast MHD model given in Horton *et al.* (1999), we show here within the framework of the hydrodynamic

approximation that there is a window of instability for $\beta_1 < \beta < \beta_2 \sim 1 - 3$ where MHD is valid and unstable for sufficiently steep pressure gradients. For $\beta > \beta_2 \gg 1$ the small $\delta W^{\rm MHD}$ values show that a kinetic variational principle must be used to determine the stability. The most serious limitations on the hydrodynamic model are (1) the neglect of the divergence of the thermal flux and (2) the neglect of the role of the charge separation arising from the divergence of the off-diagonal momentum stress tensor. With respect to global substorm dynamics, both these kinetic effects are analyzed and included in the low-dimensional simple global modeling procedure in the WINDMI substorm model of Horton and Doxas (1996, 1998). We return to this discussion after presenting a new kinetic stability theory.

The theory developed here provides theoretical support for the scenarios of substorm dynamics developed in works such as Maynard *et al.* (1996), Frank *et al.* (1998, 2000), and Frank and Sigwarth (2000). The drift waves driven by the ion pressure gradient form the precursor Pc 5 and then Pi 2 oscillations well in advance of the sudden auroral brightening in the scenarios. Integration of this microscopic description with global M-I coupling models will provide new quantitative models of substorm dynamics.

The mechanism described here theoretically has been simulated by Pritchett and Coroniti (1999) using a 3D electromagnetic particle code applied to a slowly increasing pressure gradient in a 2D equilibrium formed by the Lembége and Pellat (1982) tail field and a 2D line dipole field. A convection electric field with $E_y/B_0 = 0.1\, v_i$ was applied to produce the growing pressure gradient. In this work $B_0 \sim 20\,$nT was the model lobe field. An unstable interchange grows and saturates after mode coupling produces gradients on the scale of $k_\perp \rho_i \gtrsim 1$. The instability is localized to the transition region between the dipole field and the geotail field, consistent with the kinetic δW calculation. The present work eliminates many of the simplifications made in earlier works on the stability problem.

Here we develop and analyze kinetic stability theory for the finite β geotail flux tubes. In particular, we analyze two regimes in detail. The higher frequency modes are in the drift

wave regime where $k_\parallel v_i \simeq \omega_{bi} \lesssim \omega < \omega_{be}$ so that the ions have a local kinetic response and the electrons have a bounce-average response to the fluctuations. In this frequency range the dominant mode is the kinetic ion drift wave with $\omega_k \simeq \omega_{*pi} = k_y dp_i/en_i d\psi_y = k_y T_i/eB_n L_p$ that propagates westward and resonates with the guiding center drift velocity of ions. Here the poloidal function is $\psi(x,z) = -A_y$ the equilibrium vector potential for the nightside magnetic field $\boldsymbol{B} = -\nabla \times (\psi \widehat{\boldsymbol{y}}) = \widehat{\boldsymbol{y}} \times \nabla\psi$. As the growth rate $\gamma_k(t)$ increases, this mode continuously deforms into the MHD ballooning/interchange mode with small $E_\parallel \cong (v_A^2 k_\parallel^2 k_\perp^2 \rho_s^2/\omega_*^2) E_{k_\perp}$. The work here presents the most detailed analysis of the full compressional energy for this mode and the β-dependence of the growth rate.

The second kinetic mode is the $|\omega| < \omega_{Di}, \omega_{bi}$ low-frequency mode that is called either a convective cell or a trapped particle mode in the literature. Here we show that the compressional stabilization term dominates the energy release through the $\delta B_\parallel$ perturbation. For high plasma pressure we introduce a new expansion in powers of $1/\beta$ for finding the minimum kinetic δW. The result gives a new, analytic theory for the high beta stability of these low-frequency disturbances. Due to their low frequency and relatively large scale $k_y \rho_i \ll 1$, these modes can release substantial amounts of energy when unstable. When the modes are neutral or weakly damped, they can be driven up by nonlinear coupling to the higher frequency drift wave instabilities. Such low-frequency modes are thought to be the mechanism for producing Bohm scaling of thermal energy transport in laboratory confinement devices. To our knowledge, this work is the first study of such kinetic modes for a high β plasma with strongly curved field loops.

Sections II, III, and IV are technical calculations of the local (Sec. II) and nonlocal (Secs. III and IV) kinetic stability of a flux tube. In Sec. V we compare the results of Tsyganenko and Stern (1996) and a 2D dipole-geotail model for the stability predictions. For the modeling we choose substorms discussed by Maynard *et al.* (1996) and Frank and Sigwarth (2000) . Those not concerned with technical aspects of the stability calculations may restrict their attention to Secs. I and V, and the figures.

II. ELECTROMAGNETIC KINETIC MODE EQUATIONS

Let us start with a brief review of some features of the low-frequency waves in ae kinetic, high beta, collisionless plasma. The local kinetic modification of the three MHD waves is determined by $\omega/k_\parallel v_e$ and $\omega/k_\parallel v_i$. Recall the three modes of which one is given by $\omega^2 = k_\parallel^2 v_A^2$ with E_y dominant and the other two by $\omega_\pm^2 = (k^2/2)\{(v_A^2+v_s^2)\pm[(v_A^2+v_s^2)^2-4v_A^2v_s^2k_\parallel^2/k^2]^{1/2}\}$ with $E_x, \delta B_\parallel$ dominant for $\boldsymbol{k} = (0, k_y, k_\parallel)$. The first Alfvén mode is an ordinary wave in the limit of a weak magnetic field $(1/\beta \to 0)$. For $v_i < \omega/k_\parallel = v_A < v_e$ the Alfvén wave (A) has a weak damping rate $\gamma_A/\omega = -\frac{1}{2}(\pi T_i/T_e)^{1/2}(m_e/m_i)(v_e/v_A)(\omega/\omega_{ci})^2(\tan^2\theta + \text{cotan}^2\theta)$ where $k_\parallel = k\cos\theta$. The electric field polarization vector for $\cos\theta \ll 1$ is $\boldsymbol{e}_A = (i\omega\cos^2\theta/\omega_{ci},\ 1,\ -\omega^2v_s^2/\omega_{ci}^2v_A^2)$. The kinetic modification to the second set of modes for $\cos\theta \ll v_A/v_e$, called the magnetoacoustic (compressional Alfvén) wave (M), is $\omega^2 = k^2v_A^2 + 2(1+T_e/T_i)(k^2v_i^2)$, which gives the kinetic value of the sound speed $v_s^2 = 2(1+T_i/T_e)(T_i/m_i)$ for these waves. The polarization vector for the wave is $\boldsymbol{e}_M = (1,\ i\omega/\omega_{ci},\ -iv_s^2\omega/v_A^2\omega_{ci}\ \cos\theta)$. The damping of this wave is very weak. In the limit $B \to 0$ or equivalently $(1/\beta \to 0)$ this mode becomes the extraordinary wave.

Due to the rapid change in direction with position $\boldsymbol{x}$ of the vector $\boldsymbol{b}(\boldsymbol{x}) = \boldsymbol{B}/B$ in the geomagnetic tail and the other inhomogeneities leading to the diamagnetic drift frequencies $\omega_{*pi}, \omega_{*e}$ and to $\omega_{\nabla B}$ and ω_*, the two modes are coupled. Thus, we must present a full, symmetric 3×3 matrix for the waves in the geotail plasma. The six complex matrix elements determine the waves and their polarizations. We numerically solve the full matrix locally, and take various analytic limits to recover well-known simplified descriptions.

The coupling of the compressional Alfvén and shear Alfvén modes in a dipole field is described in Chen and Hasegawa (1991). In a weak coupling approximation they give instability conditions for the mirror $(p_\perp > p_\parallel)$ anisotropy destabilization of the compressional mode $(\delta B_\parallel \neq 0)$ and the high energy ring current resonant ion destabilization of the drift ballooning shear Alfvén mode. An energetic (E) ion component $n_E T_E \sim n_i T_i$ with $T_E/T_i \sim 10^2$ is introduced to model the ring current. The energetic drift-bounce resonance destabilizes

the modes.

Before presenting the details of the full 3×3 matrix, let us recall the low-frequency complex dielectric functions that give the dominant contributions to the wave matrix for the waves with $k_y \rho_i \ll 1$. One is the kinetic cross-field polarization drift dielectric (in mks units).

$$\epsilon_\perp \cong \sum_i \frac{m_i n_i}{B^2} \left(1 - \frac{\omega_{*pi}}{\omega}\right) \tag{1}$$

with ω_{*pi} the ion diamagnetic drift (westward) frequency, where the sum is over all ion components of the plasma. The parallel dielectric function is dominated by the electron current, is given by

$$\epsilon_\parallel \cong 1 - \frac{\omega_{pe}^2}{2k_\parallel^2 v_e^2} \left(1 - \frac{\omega_{*e}}{\omega}\right) Z' \left(\frac{\omega}{k_\parallel v_e}\right) \tag{2}$$

where Z' is the derivative of the standard plasma dispersion function. For $k_\parallel v_e/\omega \to 0$ there are $\epsilon_\parallel \cong 1 - \omega_{pe}^2/\omega^2 = 0$ plasma waves. For the slower waves of interest here with $k_\parallel v_e \gg |\omega|$, the parallel dielectric function becomes

$$\epsilon_\parallel \simeq \left(\frac{\omega_{pe}^2}{k_\parallel^2 v_e^2}\right) \left(1 - \frac{\omega_{*e}}{\omega}\right) \left(1 + i\sqrt{\frac{\pi}{2}} \frac{\omega}{|k_\parallel| v_e}\right). \tag{3}$$

The approximate dispersion relation from the full determinant $\|k^2 \delta_{ij} - k_i k_j - \omega^2 \mu_0 \epsilon_{ij}\| = 0$ approximately separates into $\left(k_y^2 \epsilon_\perp + k_\parallel^2 \epsilon_\parallel - \omega^2 \mu_0 \epsilon_\perp \epsilon_\parallel\right) = 0$ and $k_\parallel^2 = \omega^2 \mu_0 \epsilon_\perp$ modes. The result is that there are modes with

$$\omega^2 - \omega \omega_{*pi} - k_\parallel^2 v_A^2 = 0, \tag{4}$$

which at high β lead to an ion diamagnetic drift wave

$$\omega = \omega_{*pi} + \frac{k_\parallel^2 v_i^2}{\omega_{*i}\, \beta} \cong \omega_{*pi} \tag{5}$$

with a small $E_\parallel \simeq k_\perp^2 \rho_s^2 (k_\parallel^2 v_A^2/\omega_*^2) E_y$. The drift wave shear Alfvén mode has $\omega^2(1 + k_\perp^2 \rho_s^2) - \omega \omega_{*e} - k_\parallel^2 v_A^2 k_\perp^2 \rho_s^2 = 0$ with $E_\parallel \cong i\omega \delta A_\parallel \gg i k_\parallel \phi$ and becomes the low-frequency convective cell for $T_e/T_i \ll 1$ and $\beta \gg 1$. Thus, there is a mode with $\omega \cong \omega_{*pi}$ and small $E_\parallel$, and

another with $\delta j_\parallel \cong 0$ and $E_\parallel \neq 0$ at $\omega \simeq \omega_{*e}$, whereas at high β the $E_\parallel$ is dominated by the induction electric field from $\delta B_\perp$.

The symmetry of the full 3×3 wave matrix arises from the Hamiltonian structure of the wave-particle system in the phase space. A consequence of these symmetries is that there is a variational form of the perturbed energy $\mathcal{L}(\boldsymbol{U})$. Here we use the symbol $\mathcal{L}$ in order to reserve the symbol δW for the conventional potential energy release. Also, $\boldsymbol{U}$ represents any number of choices for the three potentials used to represent the perturbed electromagnetic fields. The different choices are related by gauge transformations. One choice of the three potentials is $\boldsymbol{U}_1 = (\phi, \psi, \delta B_\parallel)$ with $E_\parallel = -ik_\parallel(\phi - \psi)$ as used in Horton *et al.* (1985) and Chen and Hasegawa (1991). Here ψ is the back emf in volts from the induction electric field given by $\partial B_\perp/\partial t$ for a Faraday loop going from $y = 0$ to y in the equitorial plane and up the field line to the field point (x, y, z). A second familiar choice of fields $\boldsymbol{U}_2 = (\xi^\psi, \chi, Q_L)$ is used for the variational quadratic form in Sec. III to show the relation to the MHD potential energy $\delta W^{\rm MHD}$. Here $Q_L = \delta B_\parallel + \boldsymbol{\xi} \cdot \nabla B_0$ is the perturbed strength of the B-field in a displacement following Lagrangian frame of reference. This latter form of the potentials is convenient for going to the Kruskal-Oberman stability limit and to the ideal MHD stability limit.

In this section we use the field representation $\boldsymbol{E}_\perp = -\nabla_\perp \phi, E_\parallel = -\nabla_\parallel(\phi - \psi)$, and $\delta \boldsymbol{B} = \widehat{\boldsymbol{b}}_0 \times \nabla\psi + \widehat{\boldsymbol{b}}_0 \delta B_\parallel$. The wave matrix is a complex symmetric matrix due to the time-reversal symmetry and parity symmetry of the underlying equations. The details are given in Horton *et al.* (1985) and Chen and Hasegawa (1991), and in the FLR-fluid description in Horton *et al.* (1983). Here we summarize the key results.

A. Kinetic dispersion relation

The wave fluctuations satisfy the matrix equation $\boldsymbol{A} \cdot \boldsymbol{U} = 0$ defined by

$$\begin{bmatrix} a & b & c \\ b & d & e \\ c & e & f \end{bmatrix} \begin{bmatrix} \phi \\ \psi \\ \delta B_\parallel \end{bmatrix} = 0 \tag{6}$$

where the six complex response functions are

$$\begin{aligned} a &= -1 + \frac{T_e}{T_i}(P-1) \\ b &= 1 - \frac{\omega_*}{\omega} \\ c &= Q \\ d &= \frac{k_\perp^2 \rho_s^2 \omega_A^2}{\omega^2} - \left(1 - \frac{\omega_*}{\omega}\right) + \frac{\omega_{De}}{\omega}\left(1 - \frac{\omega_{*pe}}{\omega}\right) \\ e &= -\left(1 - \frac{\omega_{*p_e}}{\omega}\right) \\ f &= \frac{2}{\beta_e} + \frac{T_i}{T_e} R. \end{aligned} \tag{7}$$

Here the local ($|\omega| \gg k_\parallel v_i$) ion kinetic response functions P, Q, R are given by

$$\begin{aligned} P &= \left\langle \frac{\omega - \omega_{*i}(\epsilon)}{\omega - \omega_{Di}} J_0^2 \right\rangle \\ Q &= \left\langle \frac{\omega - \omega_{*i}(\epsilon)}{\omega - \omega_{Di}} \left(\frac{m_i}{b_i T_i}\right)^{1/2} v_\perp J_0 J_1 \right\rangle \\ R &= \left\langle \frac{\omega - \omega_{*i}(\epsilon)}{\omega - \omega_{Di}} \cdot \frac{m_i v_\perp^2}{b_i T_i} J_1^2 \right\rangle \end{aligned}$$

Let us consider various well-known limits. For a low β plasma, $f \gg 1$ and the determinant D of Eq. (6) is

$$D = (ad - b^2) f \simeq 0. \tag{8}$$

For this system the MHD modes have $a \simeq -b$ and $d \cong -b$. Equation (8) for $f \neq 0$ gives the kinetically modified MHD modes

$$\omega^2 - \omega\omega_{*pi} - k_\parallel^2 v_A^2 + \gamma_{\rm mhd}^2 = 0$$

and the electron drift mode

$$\omega^2(1 + k_\perp^2 \rho_s^2) - \omega\omega_{*e} - k_\parallel^2 v_A^2 k_\perp^2 \rho_s^2 = 0. \tag{9}$$

The compressional mode has $f(\omega) \simeq 0$ and is stable until the mirror mode instability condition $\beta(p_\perp/p_\parallel - 1) > C_m \approx 1$ is satisfied (Chen and Hasegawa, 1991). The details of the fluid reductions are given in Horton *et al.* (1985).

B. Bounce-Averaged Electrons

Small pitch angle electrons are either lost to the atmosphere or take such a long path that they return out of phase with the wave due to fluctuations in the intervening medium. We let f_t be the fraction of trapped electrons in the flux tube. The precise value of f_t depends on the path length allowed for coherent return and the steepness of the pitch angle gradient of the electron distribution function near the loss cone pitch angle.

1. Lost electrons have only the local adiabatic perturbed velocity distribution

$$\delta f_e = \left[\frac{e\phi}{T_e} - \left(1 - \frac{\omega_{*te}}{\omega}\right)\frac{e\psi}{T_e}\right] F_e$$

for $\lambda < \lambda_{\rm crit}$. Here $\lambda_{\rm crit}$ is the critical value of $\sin^2\alpha$ for the pitch angle α defined by the velocity vector at the magnetic equitorial plane.

2. Trapped electrons have both an adiabatic and a nonlocal bounce-averaged response:

$$\delta f_e = \left[\frac{e\phi}{T_e} - \left(1 - \frac{\omega_{*te}}{\omega}\right)\frac{e\psi}{T_e} - \left(\frac{\omega - \omega_{*e}}{\omega - \overline{\omega}_{De}}\right)\overline{K}_e\right] F_e \tag{10}$$

where

$$\overline{K}_e = \frac{1}{\tau}\oint \frac{ds}{|v_\parallel|}\left[\frac{e\phi}{T_e} - \left(1 - \frac{\omega_{De}}{\omega}\right)\frac{e\psi}{T_e} - \frac{v_\perp^2}{v_e^2}\frac{\delta B_\parallel}{B}\right]. \tag{11}$$

The electron density fluctuation is found to be

$$\frac{\delta n_e}{n_e} = \frac{e\phi}{T_e} - \left(1 - \frac{\omega_{*e}}{\omega}\right)\frac{e\psi}{T_e} - f_t\int_{t_r} d^3v\, F_e \tag{12}$$

$$\left[\frac{\omega - \omega_{*te}}{\omega - \overline{\omega}_{De}}\left(\frac{e\overline{\phi}}{T_e} - \overline{\left(1 - \frac{\omega_{De}}{\omega}\right)\frac{e\psi}{T_e}} - \overline{\frac{v_\perp^2}{v_e^2}\frac{\delta B_\parallel}{B}}\right)\right]$$

where the overbar denotes the bounce averaging $\overline{\phi} = \tau^{-1} \oint ds/|v_\parallel|\phi$, where $\tau = \oint ds/|v_\parallel|$. We will use angular brackets to denote the integral over velocity space $\langle F \rangle = \int d^3v F = 2\pi \int d\mathcal{E} d\mu/|v_\parallel| F$.

In the following section we use the dimensionless fields $e\phi/T_e \to \phi$, $e\psi/T_e \to \psi$ and $\delta B_\parallel/B \to \delta B_\parallel$.

C. Quasineutrality Condition

From the electron distribution function and δn_e in Eq. (12) and applying the condition of quasineutrality $\delta\widetilde{n}_e = \delta\widetilde{n}_i$, we find that the first row of the matrix equation becomes

$$(\boldsymbol{A}\cdot\boldsymbol{U})_1 = \widehat{a}\phi + \widehat{b}\psi + \widehat{c}\delta B_\parallel = 0,$$

where the operators $\widehat{a}, \widehat{b}, \widehat{c}$ are

$$\begin{aligned}
\widehat{a}\phi &= \left\{-1 + \frac{T_e}{T_i}(P-1)\right\}\phi + f_t \left\langle \left(\frac{\omega-\omega_{*te}}{\omega-\overline{\omega}_{De}}\right)\overline{\phi}\right\rangle \\
\widehat{b}\psi &= \left(1-\frac{\omega_{*e}}{\omega}\right)\psi - f_t\left\langle \left(\frac{\omega-\omega_{*te}}{\omega-\overline{\omega}_{De}}\right)\overline{\left(1-\frac{\omega_{De}}{\omega}\right)\psi}\ \right\rangle \\
\widehat{c}\delta B_\parallel &= Q\delta B_\parallel - f_t\left\langle \frac{(\omega-\omega_{*te})}{(\omega-\overline{\omega}_{De})}\ \overline{\frac{v_\perp^2}{v_e^2}\,\delta B_\parallel}\ \right\rangle.
\end{aligned} \tag{13}$$

For $|\omega| \gg \overline{\omega}_{De}$ we get the simplified response

$$\begin{aligned}
a &\cong -1 + f_t - f_t\,\frac{\omega_{*e}}{\omega} - f_t\,\frac{\omega_{*pe}\,\omega_{De}}{\omega^2} + \tau(P-1) \\
b &\cong 1 - \frac{\omega_{*e}}{\omega} - f_t\left(1-\frac{\omega_{*e}}{\omega}\right) \\
c &\cong Q - f_t\left(1-\frac{\omega_{*pe}}{\omega}\right).
\end{aligned} \tag{14}$$

D. Parallel Component of Ampére's Law

For $\omega^2 \gg \omega_s^2 = k_\parallel^2 c_s^2$ we obtain from Ampére's law, $\nabla_\perp^2 A_\parallel = -\mu_0 \delta j_\parallel$, the following integral-differential equation:

$$\frac{\rho_s^2 v_A^2}{\omega^2}\,\frac{\partial}{\partial s}\,\nabla_\perp^2\,\frac{\partial \psi}{\partial s} = \left[-1+\frac{\omega_{*e}}{\omega}+f_t\left\langle\left(1-\frac{\omega_{De}}{\omega}\right)g_e\right\rangle\right]\phi$$
$$+\left[1-\frac{\omega_{*e}}{\omega}-\left(1-\frac{\omega_{*pe}}{\omega}\right)\frac{\omega_{De}}{\omega}-f_t\left\langle\left(1-\frac{\omega_{De}}{\omega}\right)g_e\overline{\left(1-\frac{\omega_{De}}{\omega}\right)}\right\rangle\right]\psi$$
$$+\left[1-\frac{\omega_{*pe}}{\omega}+f_t\overline{\left(1-\frac{\omega_{De}}{\omega}\right)g_e\frac{v_\perp^2}{v_e^2}}\,\right]\delta B_\parallel \tag{15}$$

where $g_e = (\omega-\omega_{*te})/(\omega-\overline{\omega}_{De}+i0^+)$. This yields the field equation

$$(\boldsymbol{A}\cdot\boldsymbol{U})_2 = \widehat{b}\phi+\widehat{d}\psi+\widehat{e}\delta B_\parallel = 0 \tag{16}$$

where $\widehat{b}$ is the same operator as in Eq. (13) and the new operators are

$$\widehat{d}\psi = \left\{k_\perp^2\rho_s^2\,\frac{\omega_A^2}{\omega^2}-\left(1-\frac{\omega_*}{\omega}\right)+\left(1-\frac{\omega_{*pe}}{\omega}\right)\frac{\omega_{De}}{\omega}\right\}\psi \tag{17}$$
$$-f_t\left\langle\left(1-\frac{\omega_{De}}{\omega}\right)g_e\overline{\left(1-\frac{\omega_{De}}{\omega}\right)\psi}\,\right\rangle$$
$$\widehat{e}\delta B_\parallel = \left(1-\frac{\omega_{*pe}}{\omega}\right)\delta B_\parallel+f_t\left\langle\left(1-\frac{\omega_{De}}{\omega}\right)\;g_e\overline{\frac{v_\perp^2}{v_e^2}\,\delta B_\parallel}\,\right\rangle.$$

In Eq. (17), $k_\perp^2\widehat{\omega}_A^2 = -\partial_s v_A^2 k_\perp^2(s)\partial_s$ is the line-bending operator, and $\omega_e\, f_t$ is to be understood as the bounce averaging operator.

E. Radial Component of Ampére's Law

The radial (∇A) component of Ampére's law is

$$(\widehat{\boldsymbol{e}}_y\cdot\nabla)\delta B_\parallel = \mu_0\delta J_\psi = \mu_0\left(\delta J_\psi^e+\delta J_\psi^i\right) \tag{18}$$

$$\mu_0\delta J_\psi^e = \frac{ik_\theta\mu_0 neT_e}{m_i\Omega_i}\left[\left(1-\frac{\omega_{*pe}}{\omega}\right)\psi+f_t\left\langle g_e\overline{K}_e\right\rangle\right]$$

$$\mu_0\delta J_\psi^i = -\frac{ik_\theta\mu_0 n_0 eT_i}{m_i\Omega_i}\left[\tau Q\phi+R\delta B_\parallel\right]. \tag{19}$$

Thus we get the third field equation

$$(\boldsymbol{A}\cdot\boldsymbol{U})_3 = \widehat{c}\phi+\widehat{e}\psi+\widehat{f}\delta B_\parallel = 0 \tag{20}$$

where the $\widehat{f}$ operator is derived from

$$\frac{\delta B_\parallel}{B} = \delta B_\parallel = \frac{\beta_e}{2}\left[\left(1-\frac{\omega_{*pe}}{\omega}\right)\psi + f_t\left\langle \frac{mv_\perp^2}{2T_e}\, g_e \overline{K}_e \right\rangle\right] - \frac{\beta_i}{2}\left(\frac{T_e}{T_i} Q\phi + R\frac{\delta B_\parallel}{B}\right) \tag{21}$$

giving, after multiplying by $2/\beta_e$,

$$\widehat{f}\delta B_\parallel = \left(\frac{2}{\beta_e} + \frac{T_i}{T_e}\, R\right)\delta B_\parallel + \, f_t\left\langle \left(\frac{\omega-\omega_{*te}}{\omega-\overline{\omega}_{De}}\right)\frac{v_\perp^2}{v_e^2}\,\overline{\frac{v_\perp^2}{v_e^2}\,\delta B_\parallel}\right\rangle.$$

F. Reduced 2×2 Matrix Equations and Compressional Effects

The perturbative motions induced by ϕ and ψ produce a compressional change in the magnetic field $\delta B_\parallel$ given by

$$\frac{\delta B_\parallel}{B} = -\frac{1}{f}(c\phi + e\psi) \tag{22}$$

where properly $1/f$ is the inverse f^{-1} of the complicated integral operator in Eq. (21). The compressional change in the magnetic field is dictated by Amperé's law from Eq. (18) with the currents flowing across the magnetic field lines in the $\widehat{x} \propto \nabla\psi$ direction. Substituting Eq. (22) into Eqs. (19) and (20) gives the reduced 2×2 symmetric matrix

$$\begin{bmatrix} a-\dfrac{c^2}{f} & b-\dfrac{ce}{f} \\ b-\dfrac{ce}{f} & d-\dfrac{e^2}{f} \end{bmatrix}\begin{bmatrix}\phi \\ \psi\end{bmatrix} = 0. \tag{23}$$

The dispersion relation given by the determinant is

$$D_k(\omega,\mu) = ad - b^2 - \frac{1}{f}\left(c^2 d - 2bce + e^2 a\right) = 0. \tag{24}$$

The compressional MHD limit is $a \simeq -b \simeq d$, which reduces Eq. (24) to

$$ad - b^2 - \frac{d}{f}(c+e)^2 = 0. \tag{25}$$

G. Compressional terms at finite plasma pressure

To find analytically the kinetic ballooning-interchange drift mode and connect with the variational formulas, we take $\eta_e = 0$ and note $a \simeq -b \simeq d \simeq e$ for the dominant terms owing to the small $E_\parallel$. Then the full determinant D factors as

$$ad - b^2 + \frac{\tau(1-\omega_*/\omega)(Q-(1-\omega_*/\omega))^2}{\frac{2}{\beta_e}+\frac{T_i}{T_e}R} = 0 \tag{26}$$

as shown by Eq. (25). Here $\omega_{*e} = \omega_*$ for $\eta_e = 0$. The last term in Eq. (26) gives the kinetic compressional response. For the near-MHD regime, the response function ϕ in Eq. (7) reduces to

$$Q - 1 + \frac{\omega_*}{\omega} \simeq -\frac{\omega_{*pi}-\omega_*}{\omega} = -\frac{\omega_{*p}}{\omega} + i\Delta_Q \tag{27}$$

with ω_{*p} having the total pressure gradient and a small resonant part $i\Delta_Q$ from wave-particle resonance. A reasonable approximation for R in the region $\omega\omega_{Di} > 0$ is

$$R \cong c_0 \frac{[\omega - \omega_{*i}(1+2\eta_i)]}{\omega - \omega_{Di} + ic_1|\omega_{Di}|} \simeq 1 - \frac{\omega_{*i}(1+2\eta_i)}{\omega} - i\Delta_R \tag{28}$$

where c_0 and c_1 are positive fitting parameters of order $c_0 \simeq 2, c_1 \simeq 0.1$.

The resonant modes in the high-β region have

$$\omega = \omega_0 + i\gamma \simeq \omega_{*i}(1+\eta_i) + i\gamma_k \tag{29}$$

which is a westward propagating drift wave. A Taylor-series expansion of the dominant terms in Eq. (26) gives

$$\begin{aligned} ad - b^2 \simeq & \left(\frac{\omega_*}{\omega} - 1\right)\left[\frac{\omega_A^2}{\omega_0^2}\, b - b\left(1 - \frac{\omega_{*pi}}{\omega_0}\right) - \frac{\omega_*\omega_D}{\omega_0^2}\right] \\ & + \left(\frac{\omega_*}{\omega_0} - 1\right)\frac{i\gamma}{\omega_0}\left[\frac{-2\omega_A^2}{\omega_0^2}\, b - \frac{b\omega_{*pi}}{\omega_0} + \frac{2\omega_*\omega_D}{\omega_0^2}\right] \end{aligned} \tag{30}$$

for $\omega = \omega_0 + i\gamma$ with $|\gamma| \ll \omega_0$. Thus, the growth rate γ is determined by

$$\frac{i\gamma}{\omega_0}\left[\frac{2\omega_A^2}{\omega_0^2} + \frac{\omega_{*pi}}{\omega_0}\right] b + \frac{T_e}{T_i}\frac{(\omega_{*p}/\omega_0 - i\Delta_Q)^2}{c_0[1 - \frac{\omega_{*i}(1+2\eta_i)}{\omega_0} - i\Delta_R]} = 0 \tag{31}$$

for $\Delta_Q \sim \Delta_R \ll 1$. Since $\omega_{*p}/\omega_0 \gtrsim 1$ the significant resonant contribution comes from the denominator. Thus, we obtain the growth rate formula

$$\frac{i\gamma}{\omega_0}\left(\frac{2\omega_A^2}{\omega_{*p}^2} + 1\right) b + \frac{T_e}{T_i}\frac{(\omega_*/\omega_0)^2\left[\frac{-\eta_i}{1+\eta_i} + i\Delta_R\right]}{c_0\left[\left(\frac{\eta_i}{1+\eta_i}\right)^2 + \Delta_R^2\right]} = 0 \tag{32}$$

with $\gamma > 0$ for $-\Delta_R \equiv \mathrm{Im}(R) > 0$.

H. Trapped Electron Effect on MHD Stability

Here we explain the relationship between our theory and that of Cheng (1999). Cheng denotes the trapped electron (t) and untrapped (u) fractional electron densities as

$$\begin{aligned} \frac{N_{et}(s)}{N_e} &= \left(1-\frac{B(s)}{B_{\max}}\right)^{1/2} \\ \frac{N_{eu}(s)}{N_e} &= 1-\left(1-\frac{B(s)}{B_{\max}}\right)^{1/2} . \end{aligned} \tag{33}$$

In the central plasma sheet (CPS) where $B(s) \ll B_{\max}$ then $N_{eu}(s)/N_e \simeq B(s)/2B_{\max} = 1-f_t \ll 1$. Now away from $B_{\max}$ the perturbed electrons have the small untrapped density perturbation

$$\delta n_{eu} = \frac{eN_{eu}}{T_e}\left[\frac{\omega_{*e}}{\omega}\,\phi + \left(1-\frac{\omega_{*e}}{\omega}\right)(\phi-\psi)\right], \tag{34}$$

and the large, trapped density perturbation

$$\delta n_{et} = \frac{eN_{et}}{T_e}\left[\frac{\omega_{*e}}{\omega}\,\phi + \left(1-\frac{\omega_{*}}{\omega}\right)\left[\phi-\psi-\left\langle\frac{\overline{(\omega-\omega_{De})(\phi-\psi)}}{(\omega-\overline{\omega}_{De})}\right\rangle\right] + \delta\widehat{n}_{et}\right] \tag{35}$$

where

$$\delta\widehat{n}_{et} = -\int\frac{d^3v\,F_e}{T_e}\left(\frac{\omega-\omega_{*te}}{\omega-\overline{\omega}_{De}}\right)\left(\overline{\frac{\omega_{De}}{\omega}\,\phi} + \overline{\frac{v_\perp^2}{2\omega_{ce}}\,\delta B_\parallel}\right).$$

The complicated formulas (34) and (35) are known to shift the β_1 and β_2 values in Fig. 1 and may be useful for future refinement of substorms onset conditions. The perturbed ion density, following Cheng and Lui (1998) (hereafter designated C-L), is

$$\begin{aligned} \delta n_i \cong -\frac{eN_i}{T_i}&\left[\frac{\omega_{*i}}{\omega}+\left(1-\frac{\omega_{*pi}}{\omega}\right)\left(1-\overline{J_0^2}\right)\right]\phi \\ &+\frac{e}{T_i}\int d^3v\,F_i\left(\frac{\omega-\omega_{*t}}{\omega-\omega_{di}}\right)\left(\frac{\omega_{Di}}{\omega}\,J_0\phi+\frac{v_\parallel J_1\delta B_\parallel}{k_\perp}\right). \end{aligned} \tag{36}$$

The quasineutrality condition yields

$$\left(\frac{N_{eu}+N_{et}\Delta}{N_e}\right)(\phi-\psi) = -\frac{T_e}{T_i}\left(\frac{\omega-\omega_{*pi}}{\omega-\omega_{*e}}\right)(1-\Gamma_0)\phi + \frac{T_e}{eN_e}\left(\delta\widehat{n}_i-\delta\widehat{n}_e\right)$$

where $\Gamma_0 = I_0(b_i)\exp(-b_i)$ with $b_i = k_\perp^2\rho_i^2$ and $b = T_e b_i/T_i$.

Using these results in the parallel component of Amperé's law one obtains

$$\nabla_\parallel \left(k_\perp^2 \nabla_\parallel \psi\right) + \frac{\omega(\omega-\omega_{*pi})}{v_A^2}\,\frac{1-\Gamma_0}{\rho_i^2}\,\phi + \left(\frac{\boldsymbol{B}\cdot\boldsymbol{\kappa}\times\boldsymbol{k}}{B^4}\right)(2\boldsymbol{k}_\perp\cdot\boldsymbol{B}\times\nabla p)\,\phi$$
$$-\frac{\boldsymbol{B}\cdot\boldsymbol{\kappa}\times\boldsymbol{k}_\perp}{B^2}\,\omega\sum_j \delta\widehat{p}_j = 0 \tag{37}$$

where

$$\delta\widehat{p}_j = m_j\int d^3v\left(\frac{1}{2}\,v_\perp^2 + v_\parallel^2\right)F_M g_j\left[\left(1-\frac{\omega_{*ti}}{\omega}\right)\phi\left(1-J_0^2\right) + g_j\,J_0\psi\right]$$

and quasineutrality relates ψ to ϕ.

The approximate solution reduces to $\omega = \omega_{*pi}/2 + i\gamma_k^{\mathrm{C-L}}$, yielding the growth rate

$$\gamma_k^{\mathrm{C-L}} \cong \left(\gamma_{\mathrm{mhd}}^2 - k_\parallel^2 v_A^2 S\right)^{1/2} \tag{38}$$

with a stabilizing factor $S \gg 1$ from the trapped electron's "stiffening" the magnetic field lines.

We differ with Cheng and Lui (1998) due to our inclusion of $\delta B_\parallel$ as the key first-order feature of the problem. The magnetic compression in $\delta B_\parallel$ provides a large stabilizing influence over the modes that C-L view as strongly unstable when $\beta > \beta_{\mathrm{cr}}$. We find that the high β, modes have a weak resonant instability at high β given approximately by Eq. (32) and developed further in Sec. III.5.

I. Finite $E_\parallel$ in the low-β_i region

As emphasized by Cheng and Lui (1998), kinetic theory describes the finite parallel electric field from charge separation effects. The result is expressed as the polarization relation

$$\frac{E_\parallel}{(-ik_\parallel\phi)} = \frac{\phi-\psi}{\phi} \tag{39}$$

and follows from the 3×3 matrix in Eq. (6). It is useful to work out analytically the low-β, small $b_i = k_\perp^2\rho_i^2$ limit of the dispersion relation. We show that the effect is to increase the critical β_1 for the onset of modes with finite b_i. For $b_i \ll 1$ the effect is weak. Thus, for the

large-scale kinetic modes, the more important modification is from the fluctuation-ion drift resonances than from the finite $E_\parallel$. For the effect on the electrons, the $E_\parallel$ is large and their motion alone would drive $\psi \to \phi$ producing $E_\parallel = 0$, as we shall see now from quasineutrality.

From Eq. (12) for the perturbed electron density we get

$$\frac{\widetilde{n}_e}{N_e} = \frac{e\phi}{T_e} - \left(1 - \frac{\omega_{*e}}{\omega}\right)\frac{e\psi}{T_e} - f_t\left(1 - \frac{\omega_{*e}}{\omega}\right)\left[\left(\frac{e\phi}{T_e} - \frac{e\psi}{T_e}\right) + \left(\frac{\omega_{De}}{\omega}\right)\frac{e\psi}{T_e}\right]. \tag{40}$$

Two useful limits are (1) for $E_\parallel = 0$ the equation gives $\widetilde{n}_e = (\omega_{*e}/\omega)(N_e e\phi/T_e)$ and (2) for $\psi = 0$ the adiabatic electrons and trapped fraction with $(1 - \omega_{*e}/\omega)(e\phi/T_e)$ response. For the ions the well-known drift wave frequency response is electrostatic:

$$\frac{\widetilde{n}_i}{N_i} = \frac{e\phi}{T_i}\left[-\frac{\omega_{*i}}{\omega} - b_i\left(1 - \frac{\omega_{*pi}}{\omega}\right)\right].$$

Thus, quasineutrality ($\widetilde{n}_i = \widetilde{n}_e$) gives the result

$$\left(1 - \frac{\omega_{*e}}{\omega}\right)(1 - f_t)(\psi - \phi) = \frac{T_e}{T_i}\, b_i\left(1 - \frac{\omega_{*pi}}{\omega}\right)\phi \tag{41}$$

which shows that the FLR ion polarization current on the right-hand side of Eq. (41) produces the charge separation driving $E_\parallel$.

Now recall that f_t is shorthand for the integral over the phase space of the bounce averaging operator defined in Eq. (11). So if we define the eigenvalue λ_b of the averaging operator

$$\widehat{\mathcal{L}} \equiv \left\langle \frac{1}{\tau}\int \frac{ds(\cdots)}{|v_\parallel(\mathcal{E},\mu)|}\right\rangle \to \lambda_b$$

acting on the ϕ and the ψ (and these two functions have different degrees of localization in the general case so that $\lambda_{b\phi} \neq \lambda_{b\psi}$), then we can replace $f_t \to \lambda_b$. This distinction is an important one since f_t is near unity for a high value of the mirror ratio $B_{\max}/B_{\min} > 10$, while λ_b need not be so close to unity. The calculation of $\lambda_{b\phi}$ and $\lambda_{b\psi}$ is a numerical problem beyond the scope of the present work. We know from the properties of the bounce averaging operator that $0 \leq \lambda_b \leq 1$.

From Eq. (41) we may express the polarization as

$$\phi = \frac{\psi}{1 + \frac{b(1-\omega_{*pi}/\omega)}{(1-f_t)(1-\omega_{*e}/\omega)}} \tag{42}$$

where $b = b_i T_e/T_i$.

The polarization relation of Eq. (42) is convenient for seeing that modes with $\omega \approx \omega_{*e}$ (drift modes propagating eastward) can have large $\widetilde{E}_\parallel$ with $\widetilde{j}_\parallel \approx 0$. In contrast, drift modes propagating westward ($\omega \approx \omega_{*pi}$) have small $\widetilde{E}_\parallel$ compared with either $-ik_\parallel\phi$ or$-\partial\widetilde{A}_\parallel/\partial t$. That is, the inductive $E_\parallel(\psi)$ nearly cancels the charge separation $E_\parallel(\phi)$, $|\psi - \phi|/|\psi| \ll 1$.

Cheng and Lui (1998) argue that the "stiffening" factor

$$S = 1 + \frac{b(\omega - \omega_{*pi})}{(1 - f_t)(\omega - \omega_{*e})} \tag{43}$$

from the denominator of Eq. (42) is large and that this gives an increase of the Alfvén wave line bending stabilization. We argue that $f_t \to \lambda_b$ with the bounce averaging eigenvalue λ_b being not so close to unity, makes it difficult for the S-factor to be much larger than $S_{\max} \lesssim 2$. Thus, we find that the $\delta B_\parallel$-effects and the wave-particle resonances are the dominant effects determining the onset of the westward propagating drift waves.

In Figs. 3 and 4 we show the results of this section (Sec. II) applied to typical geotail flux tubes. First we use the simple formulas in Eqs. (4) and (38) that balance the pressure gradient drive with the line bending stabilization $k_\parallel^2 v_A^2 S(k_y)$. Figure 3 gives the profile of the dimensionless pressure gradient in frame (a), the dimensionless field line curvature $R_E\kappa(x, y = z = 0)$ in frame (b), and the balance of the growth rate and the line bending stabilization in frame (c) for the Tsyganenko 96 equilibrium model. Clearly, without plasma compression, the region beyond $|x| \gtrsim 7$ ($\beta > \beta_1$) is strongly unstable. Increasing S from 1 to 10 moves the unstable region tailward by about $1\,R_E$. In Fig. 4 we give the stability results for the full 3×3 determinant, which shows the high-beta stabilization of the strongly ($\gamma_k/\omega_k \lesssim 1$) unstable modes for $\beta > \beta_2$ in frame (a). The high beta region in the full kinetic description has only a resonant ion-wave pressure gradient driven instability that produces anomalous transport rather than global MHD-like motions.

Figs3,4

III. VARIATIONAL FORMS FOR THE SYSTEM'S ENERGY

Now we pursue the development of the nonlocal stability theory of these kinetic instabilities and the compressional stability condition for $\beta > \beta_2$. For understanding the relationship to ideal MHD stability theory, a convenient gauge is that in which the perturbed fields $\delta\boldsymbol{E}$ and $\delta\boldsymbol{B}$ are expressed in terms of the perpendicular component of the displacement vector $\boldsymbol{\xi}\,\exp(iky - i\omega t)$ and the electrostatic potential $\phi\,\exp(iky - i\omega t)$. The perpendicular component of the vector potential $\boldsymbol{A}_\perp$ is related to $\boldsymbol{\xi}$ by $\boldsymbol{A}_\perp = \boldsymbol{\xi} \times \boldsymbol{B}$, where $\delta\boldsymbol{B} = \nabla \times \boldsymbol{A}_\perp$ and $\delta\boldsymbol{E} = -\nabla\phi - \partial_t\,\boldsymbol{A}_\perp$.

The variational quadratic form $\mathcal{L}$ for the dynamics of the perturbed fields in these fields is

$$\mathcal{L}(\boldsymbol{\xi},\phi) = \int d^3r \left[-mN\omega^2\,\boldsymbol{\xi}\cdot\boldsymbol{\xi} + \frac{1}{4\pi}\boldsymbol{Q}_\perp\cdot\boldsymbol{Q}_\perp + \frac{1}{4\pi}Q_L Q_L - 2\boldsymbol{\xi}\cdot\nabla p(\psi)\,\boldsymbol{\xi}\cdot\boldsymbol{\kappa}\right]$$
$$+\sum\int d^3r\,d^3v\frac{\partial F_0}{\partial\mathcal{E}}\left\{e^2\phi\phi - \frac{\omega-\omega^*}{\omega-\overline{\omega}_D}\overline{K}\,\overline{K}\right\} = 0 \tag{44}$$

where $\boldsymbol{Q}$ is the perturbed magnetic field,

$$\boldsymbol{Q} = \nabla\times(\boldsymbol{\xi}\times\boldsymbol{B})\,. \tag{45}$$

Here, $Q_\parallel = \boldsymbol{b}\cdot\boldsymbol{Q}$, $\boldsymbol{Q}_\perp = \boldsymbol{b}\times(\boldsymbol{Q}\times\boldsymbol{b})$, and

$$Q_L = Q_\parallel + \boldsymbol{\xi}\cdot\nabla B - B\boldsymbol{\xi}\cdot\boldsymbol{\kappa} = -B(\nabla\cdot\boldsymbol{\xi} + 2\boldsymbol{\xi}\cdot\boldsymbol{\kappa}). \tag{46}$$

The bounce frequencies ω_b of the ions and electrons are assumed to be large compared to ω, ω_* and ω_D. With $\mu B = mv_\perp^2/2$ and $\mathcal{E} = mv^2/2$ the various quantities for $\mathcal{L}$ are as follows:

$$\begin{aligned}
K &= e\phi + \mu Q_L + (2\mathcal{E} - \mu B)\,\boldsymbol{\xi}\cdot\boldsymbol{\kappa}\\
\overline{K}(\mathcal{E},\mu) &= \frac{\int\frac{ds}{v_\parallel}K(\mathcal{E},\mu,s)}{\int\frac{ds}{v_\parallel}}\\
\boldsymbol{\kappa} &= \frac{\kappa}{B}\nabla\psi\\
\omega_* &= -\frac{k_y}{eB}\frac{\nabla y\cdot\boldsymbol{b}\times\nabla F_0}{\frac{\partial F_0}{\partial\mathcal{E}}}\\
\omega_D(\mathcal{E},\mu) &= \frac{k_y}{eB}\left(\mu\nabla y\cdot\boldsymbol{b}\times\nabla B + 2(\mathcal{E}-\mu B)\nabla y\cdot\boldsymbol{b}\times\boldsymbol{\kappa}\right)
\end{aligned} \tag{47}$$

where $\boldsymbol{b}$ is the unit magnetic field vector, $\boldsymbol{\kappa}$ the field line curvature, $p(\psi)$ the plasma pressure, $F_0(\mathcal{E})$ the equilibrium particle distribution function.

We use curvilinear coordinates ψ, y, s, where s is the coordinate measuring distance along the field line. Let the vector potential be expressed in terms of the field components A_ψ and χ as follows

$$\boldsymbol{A}_\perp = A_\psi \nabla\psi + B\nabla_\perp \frac{\chi}{B}. \tag{48}$$

from which $\boldsymbol{\xi}_\perp = \boldsymbol{b} \times \boldsymbol{A}_\perp / B$ yields

$$\boldsymbol{\xi} = \frac{A_\psi}{B}\boldsymbol{b} \times \nabla\psi + \boldsymbol{b} \times \nabla \frac{\chi}{B}. \tag{49}$$

The divergence of $\boldsymbol{\xi}$ and the curl of $\boldsymbol{A}_\perp$ for perturbations varying as $\exp(ik_y y)$ yield

$$\begin{aligned} \nabla \cdot \boldsymbol{\xi} &= ik_y A_\psi - \boldsymbol{\xi} \cdot \boldsymbol{\kappa} = ik_y A_\psi + i\frac{k_y}{B}\chi \\ \boldsymbol{Q}_\perp &= \boldsymbol{b} \times \nabla\psi \; \boldsymbol{b} \cdot \nabla \left(A_\psi + B\frac{\partial}{\partial\psi}\frac{\chi}{B} \right) + ik_y \; \boldsymbol{b} \times \nabla y \; \boldsymbol{b} \cdot \nabla\chi. \end{aligned} \tag{50}$$

We find it convenient to take ϕ, Q_L, and $\xi^\psi = \boldsymbol{\xi} \cdot \nabla\psi = -ik_y\chi$ as the independent field variables instead of ϕ, A_ψ, and χ. This introduces a kinetically correct contravariant displacement field ξ^ψ that reduces to the MHD $\xi^\psi_{\rm mhd} = X(s)$ in the fluid limit. To express all quantities in terms of ϕ, Q_L, and ξ^ψ we use the transformation

$$\begin{aligned} A_\psi &= \frac{i}{k}\left(\frac{Q_L}{B} + \frac{\kappa}{B}\xi^\psi \right) \\ \chi &= \frac{i}{k}\xi^\psi \end{aligned} \tag{51}$$

where the subscript y on k_y is dropped for simplicity

In the limit of $k \gg \kappa$, the quadratic form (44) can be approximated as

$$\begin{aligned} \mathcal{L}(\xi^\psi, Q_L, \phi) = \int \frac{ds}{B} \left[-\frac{mN\omega^2}{B^2}\,\xi^\psi\xi^\psi + \frac{1}{4\pi}\frac{\partial\xi^\psi}{\partial s}\frac{\partial\xi^\psi}{\partial s} + \frac{1}{4\pi}\,Q_L Q_L - 2\frac{\kappa}{B}\,\frac{\partial p}{\partial\psi}\xi^\psi\xi^\psi \right] \\ + \sum \int \frac{ds}{B} \int d^3v \frac{\partial F_0}{\partial\mathcal{E}} \left\{ e^2\phi\phi - \frac{\omega - \omega^*}{\omega - \overline{\omega}_D}\overline{K}\,\overline{K} \right\} = 0 \end{aligned} \tag{52}$$

where

$$K = e\phi + \mu Q_L + (2\mathcal{E} - \mu B)\frac{\kappa}{B}\xi^\psi. \tag{53}$$

and the bar denotes the bounce average.

A. Equivalence of Variational Equations and 3×3 Matrix

To demonstrate the equivalence of the matrix in Eq. (6) and the local variational equations $\delta\mathcal{L}/\delta U_\alpha = 0$, we express Eq. (52) for $\mathcal{L}$ in terms of the potentials

$$\boldsymbol{U}_1 = \left(\phi, A_\parallel = -\frac{ic}{\omega}\,\boldsymbol{b}\cdot\nabla\psi,\ \delta B_\parallel\right)$$

that were used in Sec. II. In terms of these potentials $\boldsymbol{U}_1 = (\psi, \phi, \delta B_\parallel)$, the $\mathcal{L}(\boldsymbol{U}_2)$ functional (52) in the high bounce frequency limit becomes the quadratic form

$$\begin{aligned}
&\int \frac{ds}{B}\left[\frac{c^2\,k_\perp^2}{\omega^2}(\boldsymbol{b}\cdot\nabla\psi)^2 + \delta B_\parallel^2\right] + \sum\int\frac{ds}{B}\,4\pi\int d^3v\Bigg[-\frac{q^2\phi^2}{T}\,F_0 + 2\left(1-\frac{\omega_*}{\omega}\right)\frac{q\psi}{T}\left(q\phi+\mu\delta B_\parallel\right)^2 \\
&\qquad -\frac{(\omega-\omega_*)(\omega-\omega_D)}{\omega^2}\,\frac{q^2\psi^2}{T}\,F_0\Bigg] \\
&+\sum\int\frac{ds}{B}\,4\pi\int\frac{d^3vF_0}{T}\,\frac{(\omega-\omega_*)}{(\omega-\overline{\omega}_D)}\left\{q\overline{\phi}+\mu\delta\overline{B}_\parallel - \overline{\left(1-\frac{\omega_D}{\omega}\right)q\lambda\psi}\right\}^2 = 0. \qquad (54)
\end{aligned}$$

We are able to evaluate the velocity integrals for Maxwellian F_0. Using quasineutrality, ($\sum F_0 q^2\omega_*/T = 0$), we transform Eq. (54) to a quadratic form that leads to the symmetric matrix $\boldsymbol{A}\cdot\boldsymbol{U}_1 = 0$ equation. In the analysis, we use the relation

$$\begin{aligned}
p &= \sum NT \\
\boldsymbol{b}\times(\boldsymbol{b}\cdot\nabla\boldsymbol{b}) &= \frac{1}{2B^2}\,\boldsymbol{b}\times\nabla(B^2+8\pi p) \qquad (55)\\
\boldsymbol{b}\times\boldsymbol{\kappa} &= \frac{\boldsymbol{b}\times\nabla B}{B} + \frac{4\pi}{B^2}\,\boldsymbol{b}\times\nabla p.
\end{aligned}$$

The potentials change according to

$$Q_L = \delta B_\parallel - \psi\,\frac{4\pi c}{\omega B^2}\,\boldsymbol{k}_\perp\cdot\boldsymbol{b}\times\nabla p,$$

and $\xi^\psi = -ik\psi$. The variational equations of Eq. (54) reproduce the matrix equation $\boldsymbol{A}\cdot\boldsymbol{U}_1 = 0$ used in Sec. II.

B. MHD-like stability limit

To develop the content of the general functional Eq. (52) we consider two limits. In the limit of $\phi = 0$ and $|\omega| > |\omega^*|, |\overline{\omega}_D|$, we have the following MHD-like variational expression for ω^2:

$$\omega^2 = \frac{\int \frac{ds}{B}\left\{\frac{1}{4\pi}\frac{\partial\xi^\psi}{\partial s}\frac{\partial\xi^\psi}{\partial s} + \frac{1}{4\pi}Q_L Q_L - 2\frac{\kappa}{B}\frac{\partial p}{\partial\psi}\xi^\psi\xi^\psi - \sum\int d^3v\,\frac{\partial F_0}{\partial\mathcal{E}}\,\overline{K}\,\overline{K}\right\}}{\int \frac{ds}{B}\frac{mN}{B^2}\xi^\psi\xi^\psi}. \tag{56}$$

The kinetic term is bounded from below by

$$\begin{aligned}
-\sum\frac{ds}{B}\int d^3v\,\frac{\partial F_0}{\partial\mathcal{E}}\,\overline{KK} &= \sum\frac{15NT}{8B_0}\int_0^1 d\lambda\,\frac{\left\{\int\frac{ds}{(1-\lambda B/B_0)^{1/2}}\left(\lambda Q_L/B_0 + \boldsymbol{\xi}\cdot\boldsymbol{\kappa}(2-\lambda B/B_0)\right)\right\}^2}{\int\frac{ds}{(1-\lambda B/B_0)^{1/2}}} \\
&\geq \sum\frac{15NT}{8B_0}\frac{\left\{\int_0^1 d\lambda\int\frac{ds}{(1-\lambda B/B_0)^{1/2}}\left(\lambda Q_L/B_0 + \boldsymbol{\xi}\cdot\boldsymbol{\kappa}(2-\lambda B/B_0)\right)\right\}^2}{\int_0^1 d\lambda\int\frac{ds}{(1-\lambda B/B_0)^{1/2}}} \\
&= \sum\frac{5NT}{3}\frac{\left\{\int\frac{ds}{B}\nabla\cdot\boldsymbol{\xi}\right\}^2}{\int\frac{ds}{B}}.
\end{aligned} \tag{57}$$

Note that $Q_L = -B\left(\nabla\cdot\boldsymbol{\xi} + 2\boldsymbol{\xi}\cdot\boldsymbol{\kappa}\right)$, from Eq. (46). Equation (56), with the kinetic term replaced by its bound (57), is minimized $\frac{\delta\omega^2}{\delta Q_L} = 0$ with respect to Q_L by choosing

$$Q_L = -\frac{40\pi p}{3B}\frac{\int\frac{ds}{B}\boldsymbol{\xi}\cdot\boldsymbol{\kappa}}{\int\frac{ds}{B}\left(1+\frac{20\pi p}{3B^2}\right)}. \tag{58}$$

Substituting Eq. (58) into (56), we then obtain the reduced one-field variational form

$$\omega^2 = \frac{\left\langle\left\{\frac{1}{4\pi}\frac{\partial\xi^\psi}{\partial s}\frac{\partial\xi^\psi}{\partial s} - 2\frac{\kappa}{B}\frac{\partial p}{\partial\psi}\xi^\psi\xi^\psi + \frac{20p}{3}\frac{\langle\boldsymbol{\xi}\cdot\boldsymbol{\kappa}\rangle^2}{\left\langle 1+\frac{20\pi p}{3B^2}\right\rangle}\right\}\right\rangle}{\left\langle\frac{mN}{B^2}\,\xi^\psi\xi^\psi\right\rangle} \tag{59}$$

where $\langle(\cdots)\rangle = \int ds/B(\cdots)/\int ds/B$ and $\boldsymbol{\xi}\cdot\boldsymbol{\kappa} = \xi^\psi\nabla\psi\cdot\boldsymbol{\kappa}/B^2$. Note that the bounding operator in Eq. (57) replaces the bounce averaging with an MHD-like compressional energy.

C. Ultra low-frequency energy principle

In the limit of $\phi = 0$ and $|\omega| < |\omega^*|, |\overline{\omega}_D|$ corresponding to hot particle populations, the kinetic variational form $\mathcal{L}$ in Eq. (52) can be approximated by

$$\begin{aligned}
&-\sum\int\frac{ds}{B}\int d^3v\,\frac{\partial F_0}{\partial\mathcal{E}}\,\frac{\omega^*}{\overline{\omega}_D}\,\overline{K}\,\overline{K} \\
&\quad= \frac{3}{4B_0}\sum\frac{\partial NT}{\partial\psi}\int_0^1 d\lambda\,\frac{\left\{\int\frac{ds}{(1-\lambda B/B_0)^{1/2}}\left(\lambda Q_L/B_0 + \boldsymbol{\xi}\cdot\boldsymbol{\kappa}(2-\lambda B/B_0)\right)\right\}^2}{\int\frac{ds}{(1-\lambda B/B_0)^{1/2}}\,\frac{1}{B}\left(-\frac{4\pi\lambda}{B_0}\,\frac{\partial p}{\partial\psi} + (2-\lambda B/B_0)\boldsymbol{\kappa}\cdot\nabla\psi\right)}.
\end{aligned}$$

This is bounded from below by

$$\geq \sum \frac{3}{4B_0}\frac{\partial(\mathrm{NT})}{\partial\psi}\frac{\left\{\int_0^1 d\lambda \int \frac{ds}{(1-\lambda B/B_0)^{1/2}}\left(\lambda Q_L/B_0 + \boldsymbol{\xi}\cdot\boldsymbol{\kappa}(2-\lambda B/B_0)\right)\right\}^2}{\int_0^1 d\lambda \int \frac{ds}{(1-\lambda B/B_0)^{1/2}}\frac{1}{B}\left(-\frac{4\pi\lambda}{B_0}\frac{\partial p}{\partial\psi} + (2-\lambda B/B_0)\boldsymbol{\kappa}\cdot\nabla\psi\right)}$$

$$= \frac{\partial p}{\partial\psi}\frac{\left\{\int \frac{ds}{B}\nabla\cdot\boldsymbol{\xi}\right\}^2}{\int \frac{ds}{B}\frac{1}{B^2}\left(-4\pi\frac{\partial p}{\partial\psi} + 2\boldsymbol{\kappa}\cdot\nabla\psi\right)}. \tag{60}$$

The terms involving Q_L in the quadratic form are minimized by

$$Q_L = -\frac{4\pi}{B}\frac{\partial p}{\partial\psi}\frac{\int \frac{ds}{B}\boldsymbol{\xi}\cdot\boldsymbol{\kappa}}{\int \frac{ds}{B}\frac{\boldsymbol{\kappa}\cdot\nabla\psi}{B^2}}. \tag{61}$$

It is important to note that in this low-frequency regime, the Lagrangian form for $\delta B_\parallel$ from Eq. (61) is proportional to $\partial p/\partial\psi$, which in the geotail is small compared with $\delta B_\parallel$ in Eq. (58) for higher frequency modes.

Substituting Eq. (61) into (52), the quadratic form, with the low-frequency bound used, is now reduced to the one-field stability form

$$\omega^2 = \frac{\left\langle \frac{1}{4\pi}\frac{\partial\xi^\psi}{\partial s}\frac{\partial\xi^\psi}{\partial s} - \frac{2\kappa}{B}\frac{\partial p}{\partial\psi}\xi^\psi\xi^\psi + \frac{2\partial p}{\partial\psi}\frac{\langle\boldsymbol{\xi}\cdot\boldsymbol{\kappa}\rangle^2}{\left\langle\frac{\kappa}{B}\right\rangle}\right\rangle}{\left\langle\frac{mN}{B^2}\xi^\psi\xi^\psi\right\rangle}. \tag{62}$$

Note the essential difference in the compressional stabilization terms in Eq. (59) for higher frequencies and Eq. (62) for lower frequencies.

D. The $\epsilon = 1/\beta$ expansion for high-plasma pressure modes

In the limit of $\beta > 1$, we have $v_A < v_{thi}$, and mode frequencies of the order $\omega \sim kv_A$ can be comparable to ω^* and ω_D.

To simplify our analysis, we continue to ignore finite Larmor radius effects and coupling to electrostatic perturbations ($E_\parallel = 0$), and we will discuss stability using the quadratic forms presented in previous sections. Minimization of the quadratic form Eq. (52) by variation with respect to Q_L yields the integral equation

$$\frac{Q_L}{4\pi} = \sum_a \int d^3v \frac{\partial F_a}{\partial H}\frac{\omega-\omega_{*a}}{\omega-\overline{\omega}_{Da}}\frac{\mu\int\frac{ds}{v_\parallel}\left[\mu Q_L + \boldsymbol{\xi}\cdot\boldsymbol{\kappa}(\mu B + mv_\parallel^2)\right]}{\int\frac{ds}{v_\parallel}} \tag{63}$$

for Q_L driven by $\boldsymbol{\xi}\cdot\boldsymbol{\kappa}$. In a future work we will solve the integral Eq. (63) numerically. Here, we develop the solution as an expansion in $\epsilon = 1/\beta \ll 1$ valid for high plasma-to-magnetic pressure regions. The first term involving Q_L on the right-hand side of Eq. (63) is proportional to $4\pi\Sigma\int d^3v\, F_a\mu^2/T_a = 8\pi P/B^2 = \beta \gg 1$. Expanding the solution as

$$Q_L = Q_L^{(0)} + \epsilon Q_L^{(1)}, \tag{64}$$

the lowest order solution of Eq. (63) satisfies

$$\int \frac{ds}{v_\parallel}\left[\mu Q_L^{(0)} + \boldsymbol{\xi}\cdot\boldsymbol{\kappa}(\mu B + m v_\parallel^2)\right] = 0. \tag{65}$$

The general solution of Eq. (65) is given by

$$Q_L^{(0)} = -\frac{\partial}{\partial s}\, B \int_0^s ds' \xi^\psi \left(\frac{\nabla\psi\cdot\boldsymbol{\kappa}}{B^2}\right). \tag{66}$$

The next-order solution $Q_L^{(1)}$ satisfies the integral equation

$$\frac{Q_L^{(0)}}{4\pi} = \sum\int d^3v \,\frac{\partial F_a}{\partial H}\,\frac{\omega-\omega_{*a}}{\omega-\overline{\omega}_{Da}}\,\mu^2\,\frac{\int\frac{ds}{v_\parallel}\,Q_L^{(1)}}{\int\frac{ds}{v_\parallel}}$$

which can be inverted to yield its bounce average $\overline{Q_L^{(1)}}$ as given by

$$\overline{Q_L^{(1)}} = \frac{1}{\alpha(\omega,\widehat{\omega}_*)}\,\frac{1}{4\pi^2\lambda^2}\,\frac{\partial}{\partial\lambda}\int_0^\lambda \frac{du u^{1/2}}{(\lambda-u)^{1/2}}\, Q_L^{(0)}(u(s)). \tag{67}$$

Note that $Q_L^{(0)}(s)$ is a function of $u = B_n/B$ through $B = B(s)$. The function $\alpha(\omega,\widehat{\omega}_{*a})$ is given by

$$\alpha(\omega,\widehat{\omega}_*) = \frac{15}{8}\sum_a \frac{n_a T_a}{B_n^2}\left(1-\frac{\widehat{\omega}_{*a}}{\omega}\right) \tag{68}$$

where $\widehat{\omega}_* = k_y T/q(1/n\,\partial n/\partial\psi + 2/T\,\partial T/\partial\psi)$ is an energy-averaged diamagnetic frequency.

The perturbed $\delta B_\parallel$, computed using Eq. (66) and shown in Fig. 5. For Fig. 5 the Fig5
second order differential equation describing Fast-MHD ballooning modes were solved with a shooting code for a 2D dipole with a constant-current geotail model equilibrium. The eigenfunction ξ^ψ is then used to compute $Q_L^{(0)}$ through Eq. (66). Figure 5 shows the results of this calculation for the reference parameters $k_y\rho_i = 0.3$, $T_e/T_i = 1$, and $\beta = 1$. For a specific example, the amplitude of $\xi^\psi(s=0) = X(0) = 1\,R_E{\cdot}1\,nT$ is fixed at a level which is below the nonlinear mixing length amplitude limit.

E. New reduced quadratic form

Substituting the solutions $Q_L^{(0)}$ and $Q_L^{(1)}$ into Eq. (52) yields the new reduced kinetically correct quadratic form

$$\int d\psi dy \int \frac{ds}{B}\Big[-\frac{\omega^2}{v_A^2}\left|\xi^\psi\right|^2 + \left|\frac{\partial \xi^\psi}{\partial s}\right|^2 + \left|Q_L^{(0)}\right|^2 - \frac{8\pi p' \boldsymbol{\kappa}\cdot\nabla\psi}{B^2}\left|\xi^\psi\right|^2$$
$$-4\pi\sum_a \int d^3v \,\frac{\partial F_a}{\partial H}\left(\frac{\omega-\omega_{*a}}{\omega}\right)\left|\mu\overline{Q_L^{(1)}}\right|^2$$
$$+i\pi(4\pi)\sum_a \int d^3v\,\frac{\partial F_a}{\partial H}(\omega-\omega_{*a})\delta(\omega-\omega_{Da})\left|\mu\overline{Q_L^{(1)}}\right|^2\Big] = 0. \tag{69}$$

Here ξ^ψ is the contravariant component of the displacement ($\xi^\psi = -ik_y\chi$) that is the kinetic theory generalization of the MHD displacement field $X(s)$. In Eq. (69), $v_A = B/(4\pi\rho_m)^{1/2}$ is the Alfvén speed with $\rho_m = \sum_a n_a m_a$. We have explicitly separated out the resonant particle contribution (last term) in Eq. (69).

1. Limiting case of flute-type modes

To gain insight in the meaning of the new one-field variational form we proceed as follows. In the flute mode limit ($\xi^\psi = \text{const}$), we obtain the exact expressions

$$Q_L^{(0)} = -\left(\frac{B_x'}{B}\right)\xi^\psi \tag{70}$$

$$\overline{Q_L^{(1)}} = -\frac{3}{16\pi}\left(\frac{B_x'}{B_n}\right)\frac{\xi^\psi}{\lambda\alpha(\omega,\widehat{\omega}_*)}. \tag{71}$$

For simplicity, we keep only the contribution of the ion dynamics ($T_e \ll T_i$). The quadratic form (69) becomes

$$-\omega^2\int\frac{ds}{B}\frac{n_i m_i}{B^2}\left(\xi^\psi\right)^2 + \int\frac{ds}{B}\int d^3v\left(\frac{\omega-\omega_{*i}}{\omega-\overline{\omega}_{di}}\right)\frac{\partial F}{\partial H_o}\left(\mu\overline{Q}_L^{(1)}\right)^2 = 0 \tag{72}$$

since the interchange and compressional terms cancel. Using the radius of curvature R_c from $B_x'/B_n = R_c^{-1}$, we find that the local dispersion relation (76) has the form

$$\omega^2 - \frac{1}{\beta_i}\left(\frac{v_A}{R_c}\right)^2\left(\frac{\omega}{\omega-\omega_{*i}}\right)(1+i\pi\Delta) = 0$$

where Δ is a positive-definite integral quantity representing resonance effects. There are two branches: The drift mode $\omega \approx \omega_{*i} + (v_a/R_c)^2/\beta_i\omega_{*i}(1+i\pi\Delta)$ which is unstable for $\Delta > 0$ and the very low-frequency mode $\omega \approx -(v_A/R_c)^2/\beta_i\omega_{*i}(1+i\pi\Delta)$ which is weakly damped. This simple flute mode analysis shows the need to proceed to the ballooning mode calculations.

2. Ballooning mode stability analysis

The quadratic form (73), again with only ions is

$$\int \frac{d\psi dy ds}{B}\Bigg[-\frac{n_i m_i \omega^2}{B^2}|\xi^\psi|^2 + \frac{1}{4\pi}\left|\frac{\partial \xi^\psi}{\partial s}\right|^2 - \frac{2\boldsymbol{\kappa}\cdot\nabla\psi}{B^2}\frac{\partial p}{\partial \psi}|\xi^\psi|^2$$
$$+ \frac{1}{4\pi}\left|Q_L^{(0)}\right|^2 - \frac{8}{15}\frac{B_{\min}^2}{nT}\frac{\omega}{\omega-\widehat{\omega}_*}u^{-1/2}\int_0^u d\lambda \frac{\lambda^2|W|^2}{(u-\lambda)^{1/2}} + i\pi\left(\frac{8}{15}\right)^2\left(\frac{B_{\min}^2}{n_0 T_i}\right)^2\frac{\omega^2}{(\omega-\overline{\omega}_*)}\frac{\pi}{2^{1/2}m^{3/2}}$$
$$\times\int_0^\infty dH_0 H_0^{5/2}\frac{\partial F_0}{\partial H_0}(\omega-\omega_*)\delta(\omega-\overline{\omega}_D)u^{-1/2}\int_0^u \frac{d\lambda\lambda^2|W|^2}{(u-\lambda)^{1/2}}\Bigg] = 0, \tag{73}$$

where

$$Q_L^{(0)} = -\frac{\partial}{\partial s}\left[B\int_0^s ds\,\frac{\boldsymbol{\kappa}\cdot\nabla\psi}{B^2}\,\xi^\psi\right] \tag{74}$$

$$W = \frac{1}{\pi\lambda^2}\frac{\partial}{\partial\lambda}\int_0^\lambda \frac{duu^{1/2}}{(\lambda-u)^{1/2}}\,\frac{Q_L^{(0)}}{4\pi}. \tag{75}$$

We are still in the process of solving the integral-differential equation resulting from the variation of Eq. (73) with respect to $\xi^\psi(s)$. We expect a residual, slow growth ($\gamma_k/\omega_k \ll 1$) instability in the high beta tail from Eq. (77) as shown in Fig. 4 from the local 3×3 dispersion analysis.

IV. COMPARISONS WITH EARLIER WORKS

Comparison with MHD stability for arbitrary plasma beta is most conveniently discussed using the quadratic forms described in the previous sections. The only equilibrium quantities required are the magnetic field geometry and the plasma pressure $p(\psi)$. Nevertheless it is useful to discuss approximate solutions of the plasma kinetic equations and to derive alternative criteria for MHD stability in terms of the particle drifts.

In the case of low plasma beta, the magnetic perturbation is negligible $Q_L \to 0$, and the frequency as determined by Eq. (60) for flute perturbations can be approximated by

$$\begin{aligned}\omega^2 &= -\frac{\int \frac{ds}{B}\left[2\,\frac{\kappa}{B}\,\frac{\partial p}{\partial \psi} - \sum\int d^3v\,\frac{\partial F_0}{\partial \mathcal{E}}\,\left\{\overline{(2\mathcal{E}-\mu B)\,\frac{\kappa}{B}}\right\}^2\right]}{\int \frac{ds}{B}\,\frac{mN}{B^2}} \\ &= -\frac{\frac{3N^2e^2}{2k_y^2c^2p}\int \frac{ds}{B_{mn}}\int_0^{B_0/B}\frac{d\lambda}{(1-\lambda B/B_0)}\,\overline{\omega}_\kappa\left(\frac{1}{2}\omega_{*p}-\frac{5}{4}\,\overline{\omega}_\kappa\right)}{\int \frac{ds}{B}\,\frac{mN}{B^2}}\end{aligned} \tag{76}$$

where we have expressed the numerator in terms of the plasma diamagnetic frequency ω_{*p} and the curvature drift frequency ω_κ defined by

$$\begin{aligned}\omega_{*p} &= \frac{ck_y}{eN}\,\frac{\partial p}{\partial \psi} \\ \overline{\omega}_\kappa &= \frac{ck_y p\,\kappa}{eN\,B_{\min}}\,\left(\frac{2B_{\min}}{B}-\lambda\right).\end{aligned} \tag{77}$$

Thus a necessary and sufficient condition for flute stability is

$$\int_0^1 d\lambda\left(\frac{5}{2}\,\overline{\omega}_\kappa^2 - \overline{\omega}_\kappa\,\omega_{*p}\right) > 0. \tag{78}$$

This inequality (82) represents an alternative statement of flute stability. If this inequality is satisfied, then so also is the sufficient condition determined by Eq. (63) for MHD flute stability in the limit of low plasma beta.

For high β we again use the perturbation expansion in Eq. (68) to solve for the minimizing Q_L given in Eqs. (69) and (70). The stabilizing effect of magnetic compressional energy is bounded from below:

$$\int \frac{ds}{B}\,Q_L^{(0)}\,Q_L^{(0)} \geq \frac{\left\{\int \frac{ds}{B}\,\frac{Q_L^{(0)}}{B}\right\}^2}{\int \frac{ds}{B}\,\frac{1}{B^2}} = \frac{\left(2\int \frac{ds}{B}\,\boldsymbol{\xi}\cdot\boldsymbol{\kappa}\right)^2}{\int \frac{ds}{B}\,\frac{1}{B^2}}. \tag{79}$$

Here we neglect end-point contributions when integrating by parts along the field line. Substituting this lower bound (79) into Eq. (60), we obtain the high-beta limit that replaces Eq. (78).

It is of interest to note that if there are no drift-reversed particles in the equilibrium, that is $\overline{\omega}_D > 0$ or equivalently $\overline{(2B_0/B-\lambda)\kappa} > \overline{4\pi\lambda/B\;\partial p/\partial\psi}$, then for flute perturbations

$$\frac{\left(2\int \frac{ds}{B}\,\boldsymbol{\xi}\cdot\boldsymbol{\kappa}\right)^2}{\int \frac{ds}{B}\,\frac{1}{B^2}} = \frac{3\xi^\psi\xi^\psi}{2}\,\frac{\int \frac{ds}{B}\,\kappa}{\int \frac{ds}{B}\,\frac{1}{B^2}}\int \frac{ds}{B_0^2}\int_0^{B_0/B}\frac{d\lambda}{(1-\lambda/B_0)^{1/2}}\left(2\,\frac{B_0}{B}-\lambda\right)\kappa$$
$$\geq \frac{3\xi^\psi\xi^\psi}{2}\,\frac{\int \frac{ds}{B}\,\kappa}{\int \frac{ds}{B}\,\frac{1}{B^2}}\int \frac{ds}{B_0^2}\int_0^{B_0/B}\frac{d\lambda}{(1-\lambda/B_0)^{1/2}}\,\frac{4\pi\lambda}{B}\,\frac{\partial p}{\partial\psi}$$
$$= 8\pi\xi^\psi\xi^\psi\,\frac{\partial p}{\partial\psi}\int \frac{ds}{B^2}\,\kappa \tag{80}$$

and hence

$$\frac{1}{4\pi}\int\frac{ds}{B}\,Q_L^{(0)}Q_L^{(0)} \geq 2\xi^\psi\xi^\psi\,\frac{\partial p}{\partial\psi}\int\frac{ds}{B^2}\,\kappa. \tag{81}$$

This inequality (81) implies that $\omega^2 > 0$, and therefore the flute perturbations are stable in the very high beta case if there are no drift-reversed particles in the equilibrium.

The bounding integral for the compressional energy that we give in Eq. (62) from the Schwartz inequality was derived by Rosenbluth *et al.* (1983), in applying the low-frequency kinetic energy principle of Van Dam *et al.* (1982) and Antonsen and Lee (1982). The same integral occurs in Hurricane *et al.* (1994, 1995) and in Lee and Wolf (1992).

Even though the exact forms of the compressional energies are different in the Hurricane stochastic model, the Lee and Wolf (1992) MHD calculation, and our bounce-averaged compressional energy, the *bounding* function used in all three works is the same. Let us see how this unusual situation arises. We have used ξ^ψ for the kinetic theory displacement field. In the MHD limit we change notation to $\xi^\psi \to X(s)$, following Lee and Wolf (1992) and Lee (1999), for the MHD displacement field.

In the MHD form of $W^{\rm MHD}$ from Lee and Wolf (1992) we have

$$W^{\rm MHD} = \int\frac{ds}{B}\left\{\left(\frac{\partial X}{\partial s}\right)^2 - \frac{2\mu_0\kappa_A}{B}\,\frac{dp}{d\psi}\,X^2\right\} + \frac{4\gamma\mu_0 p\left(\int\frac{X(s)\kappa_A}{B}\,\frac{ds}{B}\right)^2}{\int\frac{ds}{B}\left(1+\frac{\mu_0\gamma p}{B^2}\right)} \tag{82}$$

from their Eq. (15). They calculate flute interchange $W^{\rm MHD}(X=1)$ from Eq. (82). They then show that for any system that is interchange (flute) stable $W^{\rm MHD}_{X=1} > 0$, the ballooning mode $W^{\rm MHD}$ is bounded below by

$$W^{\rm MHD} > \int\frac{ds}{B}\left[\left(\frac{\partial X}{\partial s}\right)^2 - \frac{2\mu_0\kappa_A}{B}\,\frac{dp}{d\psi}\,X^2\right] + \frac{2\mu_0\,\frac{dp}{d\psi}\left(\int\frac{ds}{B}\,\frac{X\kappa_A}{B}\right)^2}{\left(\int\frac{ds}{B}\,\frac{\kappa_A}{B}\right)}. \tag{83}$$

We see immediately that their bounding function on the right-hand side of Eq. (83) is the same as that in Eq. (62) derived in Sec. III by carrying out the pitch angle and energy integrals exactly after using the Schwartz inequality in Eq. (60) on the low-frequency compressional energy. Lee and Wolf (1992) evaluate the bound in the right-hand side of Eq. (83) for two trial functions $X(\zeta) = \exp(-\zeta^2/\alpha^2)$ and $X = B_n^2/B^2(s)$ and find the lower bound is positive definite for the local Taylor expansion ($dp/d\psi = \text{const}$) equilibrium model.

In looking at the final formulas (Hurricane *et al.*, 1994, 1995a, 1995b) for the compressional energy contribution for the stochastic ion orbit model, we see that δW^{comp} (stochastic) is precisely the same as the last integral in Eq. (83) used for the lower bound. Thus, the stochastic model is most unstable in the deep tail region where in fact the model may be the most relevant since the Büchner-Zelenyi chaos parameter is definitely into the chaotic zone in the tail beyond $10\,R_E$ as shown in Horton and Tajima (1991). We plan to reformulate the earlier chaotic wave matrix theory of Horton and Tajima (1991) and Hernandez *et al.* (1993) for the ballooning-interchange mode to compare with the stochastic model of Hurricane *et al.* (1994, 1995). The Hurricane-Pellat model assumes that the chaotic pitch angle scattering is sufficiently strong to make the perturbed ion distribution function independent of pitch angle. The test particle modeling of Hernandez *et al.* (1993) did not have such a strong assumption. In the Hernandez *et al.* (1993) model, the chaos results in the resonance broadening of the standard wave-particle resonance functions due to the decay of the two-time velocity correlation function from the chaos.

Thus, we see that the differences in the compressional kinetic energy δW_{comp} vary with the dynamical models of (1) MHD, (2) adiabatic ion motion and (3) chaotic ion motion. The adiabatic compressional energy is the largest positive energy, while the MHD and the stochastic models compressional energies can change relative magnitudes. For the deep tail region where the stochastic model applies, δW^{stoch} is smaller than δW^{MHD}. This is because δW^{stoch} is proportional to the pressure gradient, whereas δW^{MHD} is proportional to the pressure. For the near-Earth region the situation changes, but there the adiabatic kinetic

theory is the correct theory. It is interesting, however, that the stochastic integral based on a kinetic calculation also exceeds the lower bound on the compressional energy released from the adiabatic theory. Thus, we conclude that only the kinetic formulations of the energy release give reliable thresholds for the growth rate of auroral field line flux tubes local interchanges.

With regard to the connection to the ionosphere, we note that Hameiri (1991) showed how the growth rate is reduced as the ionospheric conductance increases. The stability is not changed in the MHD problem, however.

V. OBSERVABLE CONSEQUENCES OF INSTABILITY

The immediate signatures of the instabilities calculated in Secs. II-IV are the oscillations of the electromagnetic fields and their polarizations. Thus, observations of $\delta E_y, \delta B_\perp$, and $\delta B_\parallel$ at $\omega \approx \omega_{*pi} = k_y \rho_i (v_i/L_p) \cong k_y \rho_i (2\pi/100\,\mathrm{s})$ are predicted for the substorm growth phase where the Fast-MHD mode instability condition has yet to be reached. These kinetic modes will locally flatten the x-gradient of the resonant part of the ion velocity distribution. The particle detectors would look for frequency-modulated energetic ion fluxes. The resonant ion energies $\mathcal{E}_k$ are predicted to be related to the wave frequency ω_{k_y} through $\omega_{k_y} = \overline{\omega}_{Di} \simeq \omega_{D_i}(\mathcal{E}_k/T_i)$ which weakly depends on $|k_y|$. Doxas and Horton (1999) have started test particle simulations to model the energy resolved modulated ion flux for comparison with spacecraft data.

As the wave growth rate increases by a further steepening of the Earthward gradient of the ion velocity distribution function to the point where $\gamma_k > \omega_{bi}$, the mode becomes the Fast MHD mode and releases a macroscopic energy comparable to the total energy in the local flux tube. The amount of flux in the interchanged flux tube is well identified by that small area of the auroral arc that undergoes auroral brightening and its motion measured by the VIS (Visible Imaging System) instrument on POLAR. We may use the three isolated substorms in Frank and Sigwarth (2000) for estimating the flux tube dynamics. Lui and

Murphree (1998) have evidence tying the substorm onset to auroral flux tubes.

In Fig. 6 the latitudinal dependence and magnetic local time dependence of (a) the flux tube volume, (b) the magnetic equitorial plane crossing point x for $z = 0$ of the flux, (c) the length $L_\parallel$ of the flux tube and (d) the locus of the central field line projected on the X-Y plane as the latitude varies from 58° to 72°. One pair of curves is for fields in the midnight meridian with $B_{IMF} = \pm 10\, nT$ and the second pair is for field lines at MLT of 2200 hrs where substorm auroral brightening occurs most frequently. The solar wind dynamic pressure is 10 nPa for all cases shown. Fig6

The auroral activation physics and the integration of these stability results into the WINDMI substorm model occurs through parallel current-voltage relationships for the auroral flux tubes. Before instability there is a steady field-aligned upward current $j_\parallel$ associated with the parallel potential drop $\Delta\phi_\parallel = \phi_i - \phi_{ms} > 0$. With onset of the flux tube convection velocity $v_x = d\xi_r/dt \cong \gamma\xi_r$, there are neighboring flux tubes separated by π/k_y with opposite signs of $\delta j_\parallel$ and thus $\delta\phi_\parallel$. The tubes with a sign of the potential fluctuation $\delta\phi_\parallel$ such as to increase the electron precipitation produce an immediate ($\leq 10\,$s) auroral brightening. The area of the auroral brightening and its westward motion and northward motion give a visualization of the nonlinear dynamics of the flux tubes within seconds. We may expect that there are numerous oscillations at $\omega_{*pi}/2\pi \sim$ Pc 4 (7-22 mHz) and Pc 5 (2-7 mHz) frequencies, and then in the last e-folding period $1/\gamma \sim 100\,$s the nonlinear motion and brightening of the flux tube takes place.

First we review one set of observations that clearly point to the kinetic interchange driftwave mechanism. Then we estimate the voltage $\delta\phi_\parallel$ from the size of a typical aurora brightening in Frank *et al.* (1998, 2000). We use Tsyganenko (1996) to calculate the energy components of δW for different flux tube footprints and solar wind parameters.

Maynard *et al.* (1996) describe the substorm onset scenario derived from a detailed analysis of six events drawn from 20 substorms. A complete array of particle and field measurements were assembled primarily from the CRRES satellite. The correlated ground

magnetometer's data for the AL index and the Pi 2 (2-25 mHz) pulsations were analyzed. The substorm onset time defined by the sharp decrease of the AL index from the rapid growth of the westward electrojet current. Prior to this onset from the AL signal, Maynard *et al.* (1996) report oscillations (periods of 2-3 min) about the mean westward $E_y(t)$ with evidence for the rippling of the inner edge of the plasma sheet. Pi 2 oscillations begin up to 20-26 min before the AL signal of the sharp increase in the westward electrojet. Thus, there would be 10-13 oscillations of a 2 minute wave, for example.

CRRES revolution 540 on 4 March 91 is discussed as a candidate for the interchange-ballooning substorm mechanism. In this event irregular E_y oscillations start at 1915 UT 25 min prior to the maximum of westward electrojet current $-$AL at 1941 UT. The onset time is given as 1938 UT where the AL first starts its sharp drop. In the period between 1915 UT to 1938 UT there are 10 or more oscillations in $E_y(t)$ about its mean value.

Six peaks of negative $E_y = \overline{E}_y + \delta E_y$ of a few mV/m are specifically labeled in Fig. 6 of Maynard *et al.* (1996). In that work the oscillations of E_y are inferred to ripple the near edge of the plasma sheet. The hypothesis is advanced that the oscillations and the rippling are manifestations of the mechanism proposed by Roux *et al.* (1991) for the interchange substorm mechanism. The theory developed here gives a modern, complete calculation of this collisionless, high-pressure plasma dynamics for substorm onset.

Now we estimate the maximum energy release and the increase in the parallel potential $\delta\phi_\parallel$ drop associated with auroral brightening from precipitating electrons from the ballooning interchange flux tube motion. The nonlinear magnitude of $\delta\phi$ is of order the magnetospheric electron temperature and increases with the local ion pressure gradient.

From Frank and Sigwarth (2000), the area of the footprint of the flux tube in the auroral region is roughly $A = (100\,\mathrm{km})^2 = 10^{10}\,\mathrm{m}^2$, so that the flux is $d\Psi = 5.8 \times 10^5\,\mathrm{Wb}$. As the auroral brightening grows in size, the flux increases up to $10^7\,\mathrm{Wb}$. Using the Tsyganenko model we can calculate the flux tube volume $V = \int ds/B \simeq 10\,R_E/50\ \mathrm{nT} \simeq 4 \times 10^{15}\,\mathrm{m/T}$ so that the total energy in the flux tube with a 10 nPa pressure is $pV d\Psi = 10^{-8}\,\mathrm{J/m^3}\cdot$

$4 \times 10^{21}\,\mathrm{m}^3 \cong 2 \times 10^{12}\,\mathrm{J}$ and grows to $4 \times 10^{13}\,\mathrm{J}$ in a few minutes. If the interchange motion occurs in $1/\gamma = 100\,\mathrm{s}$ and releases 10% of the total flux tube energy, we have a power of 40 GW released in a transient. While this power is less than the energies and powers associated with other substorm processes, it appears to explain the local dynamics. The importance of the unstable motion is that it produces a potential variation $\delta\phi$ that varies both across the field and along the field line. The cross-field variation is estimated from $\delta E_y = \gamma \xi_r B_n$ with $\xi_r \sim R_E$ to obtain $\delta E_y \leq 3\,\mathrm{mV/m}$. The potential fluctuation is then $\delta\phi = \delta E_y/k_y \lesssim 2\rho_i E_y \lesssim 500\,\mathrm{V}$. For $k_y\rho_i = 0.5$. Then parallel electric field is $\delta E_\parallel \sim \frac{1}{2}\,\delta\phi/L_\parallel \simeq 300\,\mathrm{V}/3\,R_E \sim 15\,\mu\mathrm{V/m}$. This potential drop is sufficient to produce a large $\delta j_\parallel \sim 2\,\mu\mathrm{A/m}^2$ current surge of precipitating electrons into the ionosphere. As the growth becomes nonlinear (in the last e-folding), the visible ($\delta\phi < 0$) flux tube moves tailward and westward due to the nonlinear flux tube motion. This nonlinear dynamics is complex and must be considered in numerical simulations as stated by Hurricane *et al.* (1997a,b, 1999). Hurricane *et al.* report that the motion can be nonlinearly unstable, which produces a super-accelerated motion that they call the detonation effect. The 3D simulations of Pritchett and Coroniti (1999) do not exhibit a super-accelerated motion. The flux tube motions tend to terminate in the simulation producing a thin transition layer between the displaced and undisturbed magnetospheric plasmas. This situation is described by Beklemishev (1991) for laboratory plasmas with the equivalent of a constant B_y field.

For an estimate of the potential energy released in the unstable motion and the competing stabilizing energy changes we calculate the δW components for the finite amplitude displacement $\xi^\psi = B\xi_r = 1\,nT \cdot 1\,R_E$ thought to be near the nonlinear limit. The results are shown in Fig. 7 where panel (a) shows the energy per unit of flux required to bend the Fig7
field lines, (b) the kinetic energy per unit of flux for a reference angular frequency of one hertz, (c) the energy required by kinetic (blue) and MHD (red) theories to compress the plasma, (d) the energy released by the interchange, (e) the total potential energy δW from the sum of frames (a), (c) and (d) and finally (f) the total potential energy divided by the

reference kinetic energy (b) that yields the square of the growth rate where negative and the oscillation frequency (squared) where positive.

We see that the sum of the line bending stabilization in frame (a) and the compressional stabilization in frame (c) leave a window in the transitional region of weak stabilization. The energy released from the pressure gradient times the curvature of the field line drops off in going past $10\,R_E$ into the geotail. Thus, the total potential energy δW shows the minimum in Fig. 7(f) in the transitional region. For this particular flux tube and solar wind parameters we needed to increase the average Tsyganenko 1996 pressure gradient (given by $\frac{dP}{dx} = j_y B_z$) by a factor of six to get the substantial negative values of $\omega^2 = -\gamma^2$ shown at $x = -6$ to $-7\,R_E$ in Fig. 7(f). For this flux tube the footprint is at 62° latitude and MLT 2400 hrs. The increase in the pressure required is thought to reflect the fact that during average conditions the plasma gradient adjusts to a near marginal gradient given $\delta W \simeq 0$ in this region. After a period of enhanced Earthward convection the gradient builds up exceeding the critical gradient, roughly given by Eq. (82), and the growing Pc 5 oscillations begin. During the last e-folding the auroral brightening at the footprint in the ionosphere occurs along with a motion of the flux tube.

A powerful, but simple approach to the nonlinear motion that we prefer is to use a coupled low order system of differential equations (Horton *et al.*, 1999). This system has a rich range of behavior that has not been fully explored for the nonlinear ballooning interchange mode. For large amplitude motion the low-order models (LOMS) predict nonlinear oscillations going into chaotic pulsations not unlike the transitions from Pc 5 to Pi 2 signals. The LOMS also predict the creation of sheared dawn-dusk flows (Hu and Horton, 1997). We believe that the predictions with LOMS for the M-I coupling processes and the nonlinear dynamics can be carried out with respect to an assessment of the model, and may be used to resolve the issues arising from simulations and the POLAR observations.

Acknowledgments

This work was supported by the National Science Foundation Grant ATM-9907637 and the U.S. Dept. of Energy Contract No. DE-FG03-96ER-54346.

Appendix: Kinetic ballooning instabilities:

Magnetic field structure and guiding center drift velocities

A very useful model for the geomagnetic tail system, valid quantitatively up to geosynchronous orbit, is the linear superposition of the 2D dipole and uniform current sheet ($j_y =$ const) magnetic fields. Since the model is translationally invariant in y, the eigenmodes are strictly sinusoidal in the y-direction, which greatly simplifies the stability problem. Likewise the exact particle orbits are described by a two-degrees-of-freedom Hamiltonian with effective potential $U_{\rm eff} = \left(P_y - q\,A_y(x,z)\right)^2/2m + q\phi(x,z)$. The guiding center orbits also simplify considerably, yet show the small loss cone angle $\alpha_{\ell c} = 1/(R-1)^{1/2}$ due to the large mirror ratio $R = B_{\rm ion}/B_{gt}$. One can move the ionosphere out to perhaps $3\,R_E$ in the analogous system to make the model fields closer to those of the 3D magnetosphere. The parameters of the 2D model are $B_0\,r_0^2$, B_x', and B_n, which can be optimized with respect to a given space region $\Omega = L_x L_y L_z$ for the best representation of the 3D fields. The analytical and numerical advantages of the 2D model are clear. The particle simulations of Prichett *et al.* (1997a,b) are performed in such 2D systems with further compressions of the space-time scales by use of small ion-to-electron mass ratios.

The 2D magnetotail model is derived from $\boldsymbol{B} = \nabla \times (A_y\,\widehat{\boldsymbol{y}}) = \nabla A_y \times \widehat{\boldsymbol{y}}$ with

$$A_y(x,z) = -\frac{B_0 r_0^2 x}{x^2+z^2} - \frac{1}{2}\,B_x' z^2 + B_n x. \tag{A1}$$

This gives

$$B_z(x,z) = B_n + \frac{B_0 r_0^2 (x^2-z^2)}{(x^2+z^2)^2} \tag{A2}$$

$$B_x(x,z) = B_x' z - \frac{2B_0 r_0^2 xz}{(x^2+z^2)^2} \tag{A3}$$

with

$$B^2 = B_n^2 + B_x'^2 z^2 + \frac{2B_0 r_0^2 [B_n(x^2-z^2) - 2B_x' x z^2]}{(x^2+z^2)^2} + \frac{\left(B_0 r_0^2\right)^2}{(x^2+z^2)^2}. \tag{A4}$$

The shear matrix $\partial B_i/\partial x_j$ of the magnetic field is

$$B_{x,x} = \frac{2B_0 r_0^2 z(3x^2-z^2)}{(x^2+z^2)^3} \tag{A5}$$

$$B_{x,z} = B'_x - \frac{2B_0 r_0^2 x(x^2-3z^2)}{(x^2+z^2)^3} \tag{A6}$$

$$B_{z,x} = \frac{-2B_0 r_0^2 x(x^2-3z^2)}{(x^2+z^2)^3} \tag{A7}$$

$$B_{z,z} = \frac{2B_0 r_0^2 z(z^2-3x^2)}{(x^2+z^2)^3} \tag{A8}$$

From Eqs. (A5)-(A8) we check that $\nabla \cdot \boldsymbol{B} = 0$ and see that $\mu_0 j_y = B_{x,z} - B_{z,x} = B'_x$. In the region $x^2 \gg z^2$ of the deep tail model with constant parameters, B'_x and B_n are now modified to have

$$\begin{aligned} B'_x &\to B'_x - \frac{2B_0 r_0^2}{x^3} \\ B_n &\to B_n + \frac{B_0 r_0^2}{x^2} \end{aligned} \tag{A9}$$

where we note that $x < 0$ in the nightside region of interest.

Curvature drift velocity

Now we compute the curvature vector $\boldsymbol{\kappa} = (\boldsymbol{b}\cdot\nabla)\boldsymbol{b}$ and the curvature and grad-B drift velocities. The curvature vector is

$$\boldsymbol{\kappa} = (\boldsymbol{b}\cdot\nabla)\boldsymbol{b} = \kappa_x \widehat{\boldsymbol{x}} + \kappa_z \widehat{\boldsymbol{z}}$$

with

$$\kappa_x = \frac{B_x B_{x,x} + B_z B_{x,z}}{B^2} - \frac{B_x}{2B^4}(\boldsymbol{B}\cdot\nabla)B^2 \tag{A10}$$

$$\kappa_z = \frac{B_x B_{z,x} + B_z B_{z,z}}{B^2} - \frac{B_z}{2B^4}(\boldsymbol{B}\cdot\nabla)B^2 \tag{A11}$$

and the curvature drift velocity is proportional to

$$\boldsymbol{B}\times\boldsymbol{\kappa} = \left[-\frac{B_x^2}{B^2}B_{z,x} + \frac{B_z^2}{B^2}B_{x,z} + \frac{B_x B_z}{B^2}(B_{x,x} - B_{z,z})\right]$$

or

$$\begin{aligned} B^2(\boldsymbol{B}\times\boldsymbol{\kappa})_y = &\left(B_n + \frac{B_0 r_0^2(x^2-z^2)}{r^4}\right)^2 \left(B'_x - \frac{2B_0 r_0^2 x(x^2-3z^2)}{r^6}\right) \\ &- \left(B'_x z - \frac{2B_0 r_0^2 xz}{r^4}\right)^2 \left(\frac{2B_0 r_0^2 x(3z^2-x^2)}{r^6}\right) \\ &- \left(B_n + \frac{B_0 r_0^2(x^2-z^2)}{r^4}\right)\left(B'_x z - \frac{2B_0 r_0^2 xz}{r^4}\right)\frac{4B_0 r_0^2 z(3x^2-z^2)}{r^6} \end{aligned} \tag{A12}$$

where $r = (x^2 + z^2)^{1/2}$. The curvature drift is in the y-direction and given by Eq. (A12) substituted into

$$v_{\rm curv}(x, z, v_\parallel) = \frac{m v_\parallel^2}{qB^2}(\boldsymbol{B} \times \boldsymbol{\kappa})_y. \tag{A13}$$

In the limit $z^2/x^2 \to 0$ the curvature drift reduces to

$$v_{\rm curv} = \frac{m v_\parallel^2}{q B_z^2(x)} \left(B_x' - \frac{2B_0 r_0^2}{x^3} \right). \tag{A14}$$

Gradient-B drift velocity

The gradients of B^2 are given by

$$\begin{aligned}
\frac{\partial B^2}{\partial x} &= -\frac{4B_0^2 r_0^4 x}{r^6} + \frac{4B_0 r_0^2}{r^6}\left[B_n x(B_z^2 - x^2) - B_x' z^2(z^2 - 3x^2)\right] \\
\frac{\partial B^2}{\partial z} &= 2B_x'^2 z - \frac{4B_0^2 r_0^4 z}{r^6} - \frac{4B_0 r_0^2}{r^6}\left[B_n z(z^2 - 3x^2) - B_x' z(x^2 - 3x^2)\right]
\end{aligned} \tag{A15}$$

The gradient-B drift velocity becomes

$$\begin{aligned}
v_{\nabla B}(x, z, v_\perp^2) = \frac{m v_\perp^2}{2qB^4}\left[\left(B_n + \frac{B_0 r_0^2(x^2 - z^2)}{r^4}\right)\right]\Big(-\frac{2B_0^2 r_0^4 x}{r^6} + \frac{2B_0 r_0^2}{r^6} \\
\left[B_n x(3z^2 - x^2) - B_x' z^2(z^2 - 3x^2)\right]\Big) \\
-z^2\left(B_x' - \frac{2B_0 r_0^2 x}{r^4}\right)\left[B_x'^2 - \frac{2B_0^2 r_0^4}{r^6} - \frac{4B_0 r_0^2}{r^6}\left(B_n(z^2 - 3x^2) - B_x'(x^2 - 3z^2)\right)\right].
\end{aligned} \tag{A16}$$

In the region $z^2/x^2 \ll 1$ the grad-B drift velocity reduces to

$$v_{\nabla B} = \frac{m v_\perp^2}{2qB}\left[-\frac{2B_0^2 r_0^4}{B^2 x^5} - \frac{2B_0 r_0^2 B_n}{B^2 x^3} - \frac{z^2 B_x'^3}{B^3}\right] \tag{A17}$$

where the first two terms are in the positive $\widehat{y}$ direction and the last term is in the negative $\widehat{\boldsymbol{y}}$ direction.

REFERENCES

[1] Antonsen, T.M., and Y.C. Lee, Electrostatic modification of variational principles for anisotropic plasmas, *Phys. Fluids, 25*, 132, 1982.

[2] Beklemishev, A.D., Nonlinear saturation of ideal interchange modes in a sheared magnetic field, *Phys Fluids B, 3*, 1425, 1991.

[3] Bhattacharjee, A., Z.W. Ma, and X. Wang, Ballooning instability of a thin current sheet in the high-Lundquist-number magnetotail, *Geophys. Res. Lett., 25*, 861, 1998.

[4] Chen, L., and A. Hasegawa, Kinetic theory of geomagnetic pulsations, 1, Internal excitations by energetic particles, *J. Geophys. Res., 96*(A2), 1503-1512, 1991.

[5] Cheng, C.Z., and A.T.Y Lui, Kinetic ballooning instability for substorm onset and current disruption observed by AMPTE/CCE, *Geophys. Res. Lett., 25*, 4091, 1998.

[6] Doxas, I., and W. Horton, Magnetospheric dynamics from a low-dimensional nonlinear dynamics model, *Phys. Plasmas, 6*, 2198, 1999.

[7] Frank, L.A., J.B. Sigwarth, and W.R. Paterson, High-resolution global images of Earth's auroras during substorms, in *Substorms-4*, eds. S. Kokubun and Y. Kamide, pp. 3-8, Kluwer Acad., Norwell, Mass., 1998.

[8] Frank, L. A. and Sigwarth, J. B., Findings concerning the positions of substorm onsets with auroral images from the Polar spacecraft, *J. Geophys. Res., 105*(A6), 12,747-12,761, 2000.

[9] Frank, L.A., W.R. Paterson, J.B. Sigwarth, and S. Kokubun, Observations of magnetic field dipolarization during auroral substorm onset *J. Geophys. Res., 105*(A7), 15,897, 2000.

[10] Hameiri, E., and M.G. Kivelson, Magnetospheric waves and the atmosphere-ionosphere layer, *J. Geophys. Res., 96*(A12), 21,125-21,134, 1991.

[11] Hernandez, J., W. Horton, and T. Tajima, Low-frequency mobility response functions for the central plasma sheet with application to tearing modes, *J. Geophys. Res., 98*, 5893, 1993.

[12] Horton, W., H.V. Wong, and J.W. Van Dam, Substorm trigger condition, *J. Geophys. Res., 104*, 22745, 1999.

[13] Horton, W., and I. Doxas, A low-dimensional dynamical model for the solar wind driven geotail-ionosphere system, *J. Geophys. Res., 103A*, 4561, 1998.

[14] Horton, W., H. V. Wong, and R. Weigel, Interchange trigger for substorms in a nonlinear dynamics model, *Phys. Space Plasmas, 15*, 169, 1998.

[15] Horton, W., and I. Doxas, A low-dimensional energy conserving state space model for substorm dynamics, *J. Geophys. Res., 101*, 27,223-27,237, 1996.

[16] Horton, W., and T. Tajima, *J. Geophys. Res., 96*, 15811, 1991.

[17] Horton, W., J.E. Sedlak, D.-I. Choi, and B.-G. Hong, *Phys. Fluids, 28*, 3050, 1985.

[18] Horton, W., D.-I. Choi, and B.G. Hong, *Phys. Fluids, 26*, 1461, 1983.

[19] Hu, G., and W. Horton, Minimal model for transport barrier dynamics based on ion-temperature-gradient turbulence, *Phys. Plasmas, 4*(9), 3262-3272, 1997.

[20] Hurricane, O.A., R. Pellat, and F.V. Coroniti, The kinetic response of a stochastic plasma to low-frequency perturbations, *Geophys. Res. Lett., 21*, 4253, 1994.

[21] Hurricane, O.A., R. Pellat, and F.V. Coroniti, The stability of a stochastic plasma with respect to low-frequency perturbations, *Phys. Plasmas, 2*, 289, 1995a.

[22] Hurricane, O.A., R. Pellat, and F.V. Coroniti, A new approach to low-frequency "MHD-like" waves in magnetospheric plasmas, *J. Geophys. Res., 100*, 19,421-19,428 1995b.

[23] Hurricane, O.A., R. Pellat, and F.V. Coroniti, Instability of the Lembége-Pellat equi-

librium under ideal magnetohydrodynamics, *Phys. Plasmas, 3*, 2472, 1996.

[24] Hurricane, O.A., MHD ballooning stability of a sheared plasma sheet, *J. Geophys. Res., 102*, 19,903, 1997a.

[25] Hurricane, O.A., B.H. Fong, and S.C. Cowley, Nonlinear magnetohydrodynamic detonation: Part I, *Phys. Plasmas, 4*, 3565, 1997b.

[26] Hurricane, O.A., B.H. Fong, S.C. Cowley, F.V. Coroniti, C.F. Kennel, and R. Pellat, Substorm detonation, *J. Geophys. Res., 104*(A5), 10,221, 1999.

[27] Kruskal, M.D., and C.R. Oberman, On the stability of plasma in static equilibrium, *Phys. Fluids, 1*, 275, 1958.

[28] Lee, D.-Y., Effect of plasma compression on plasma sheet stability, *Geophys. Res. Lett., 26*, 2705, 1999.

[29] Lee, D.-Y., Ballooning instability in the tail plasma sheet, *Geophys. Res. Lett., 25*, 4095, 1998.

[30] Lee, D.-Y., and R.A. Wolf, Is the Earth's magnetotail balloon unstable? *J. Geophys. Res., 97*, 19,251-19,257, 1992.

[31] Lembége, B., and R. Pellat, Stability of a thick two-dimensional quasineutral sheet, *Phys. Fluids, 25*, 1995, 1982.

[32] Lui, A.T.Y., and J.S. Murphree, A substorm model with onset location tied to an auroral arc, *Geophys. Res. Lett., 25*, 1269-1272, 1998.

[33] Lui, A.T.Y., P.H. Yoon, and C.-L. Chang, Quasilinear analysis of ion Weibel instability in the Earth's neutral sheet, *J. Geophys. Res., 98*, 153, 1993.

[34] Lyons, L.R., A new theory for magnetospheric substorms, *J. Geophys. Res., 100*, 19,069, 1995.

[35] Maynard, N.C., W.J. Burke, E.M. Basinska, G.M. Erickson, W.J. Hughes, H.J. Singer, A.G. Yahnin, D.A. Hardy, and F.S. Mozer, Dynamics of the inner magnetosphere near times of substorm onsets, *J. Geophys. Res., 101*, 7705-7736, 1996.

[36] Pritchett, P.L., and F.V. Coroniti, Drift ballooning mode in a kinetic model of the near-Earth plasma sheet, *J. Geophys. Res., 104*, 12,289-12,299, 1999.

[37] Pritchett, P.L., and F.V. Coroniti, Interchange and kink modes in the near-Earth plasma sheet and their associated plasma flows, *Geophys. Res. Lett., 24*, 2925-2928, 1997.

[38] Rosenbluth, M.N., and C.L. Longmire, Stability of plasmas confined by magnetic fields, *Ann. Phys., 1*, 120, 1957, 1983.

[39] Rosenbluth, M.N., S.T. Tsai, J.W. Van Dam, and M.G. Engquist, Energetic particle stabilization of ballooning modes in tokamaks, *Phys. Rev. Lett., 51*, 1967, 1983.

[40] Roux, A., S. Perrault, P. Robert, A. Morane, A. Pedersen, A. Korth, G. Kremser, B. Aparicio, D. Rodgers, and R. Pellinen, Plasma sheet instability related to the westward traveling surge, *J. Geophys. Res., 96*, 17,697-17,714, 1991.

[41] Sagdeev, R.Z., V.D. Shapiro, and V.I. Shevchenko, Convective cells in plasmas, *Fiz. Plazmy, 4*, 551, 1978.

[42] Smith, J.P., J.-L. Thiffeault, and W. Horton, Dynamical range of the WINDMI model: An exploration of possible magnetospheric plasma states, *J. Geophys. Res., 105*, 12983, 2000.

[43] Sundaram, A. K., and D.H. Fairfield, Stability of resistive MHD tearing and ballooning modes in the tail current sheet, *J. Geophys. Res., 102*(AA9), 19,913-19,926, 1997.

[44] Toffoletto, F.R., R.W. Spiro, R.A. Wolf, M. Hesse, and J. Birn, Self-consistent modeling of inner magnetospheric convection, in *Third International Conference on Substorms (ICS-3)*, eds. E.J. Rolfe and B. Kaldeich, pp. 223-230, Eur. Space Agency Pub. Div.,

Noordwijk, Netherlands, 1996.

[45] Tsyganenko, N.A., and D.P. Stern, Modeling of the global magnetic field of the large-scale Birkeland current systems, *J. Geophys. Res., 101*, 27187-27198, 1996.

[46] Van Dam, J.W., M.N. Rosenbluth, and Y.C. Lee, A generalized kinetic energy principle, *Phys. Fluids, 25*, 1349, 1982.

FIGURE CAPTIONS

FIG. 1. Sketch showing the relationship between the $\delta W^{\rm MHD}$ computed from the mathematical minimization of the ideal MHD model over all trial functions and the minimization δW (Fast) which takes into account the physical condition for applicability of MHD. The stabilization of the MHD for $\beta > \beta_2$ is due to compression of the plasma in the flux tubes which requires kinetic theory for a precise evaluation.

FIG. 2. A comparison of the simple MHD equilibrium constructed from a 2D dipole and a constant $j_y = dp/d\psi_y$ current sheet (dashed green curve) with one setting for the standard empirical model (Tsyganenko 96). Panel (a) shows the $B_z(x)$ profiles. Panel (b) shows the pressure profile obtained from axial force balance $dp/dx = j_y B_z$. Panel (c) shows the current density comparison. Panel (d) shows the plasma pressure to the magnetic pressure $\beta(x) = 2\mu_0 p(x)/B_z^2(x)$ along the nightside geotail axis. The parameters chosen for the model are $B_0 r_0^2 = 3085$, $B_x' = 15.0$, and $B_n = 0.3$. The conditions used for Tsyganenko 96 are $P_{\rm dyn} = 3.0\,nPa$, $D_{\rm st} = -50\,nT$, $B_y^{\rm IMF} = 0.0$, and $B_z^{\rm IMF} = -10.0$ nT.

FIG. 3. The logarithmic pressure gradient $R_E/L_p = p^{-1}(dp/dx)$ (a), the dimensionless radius of curvature $\kappa(x) = \widehat{\boldsymbol{e}}_x \cdot (\widehat{\boldsymbol{b}} \cdot \nabla)\widehat{\boldsymbol{b}}$ (b), the maximum growth rate $\gamma_{\rm max} = v_{ti}/(L_p R_c)^{1/2}$ (c) where $\kappa(x) = 1/R_c(x)$ and v_{ti} was taken as 300 km/s corresponding to 1 kev protons, and the Alfvén frequency $B/(L_\parallel \sqrt{\mu_0 \rho_m})$ where ρ_m was taken from a Lysak model for the density and $L_\parallel$ was taken as $3/\kappa_x$. All quantities were computed from Tsyganenko 96 with the conditions, $P_{\rm dyn} = 3.0nPa$, $D_{\rm st} = -50nT$, $B_y^{\rm IMF} = 0.0$, and $B_z^{\rm IMF} = -10.0nT$.

FIG. 4. The local kinetic theory growth rate computed from the full 3×3 determinant in Eq. (26) as a function of β. Here $k_y\rho_i = 0.3$, $T_e/T_i = 1$ and $L_p/R_c = 1$ and the figure shows that the critical values β_1 and β_2 are still well defined. However, due to the ion kinetic resonances $\omega_\kappa = \omega_{Di}(\epsilon)$ there is a residual kinetic instability for

$\beta > \beta_2$. The unstable mode has an MHD-like polarization (with $\psi/\phi = 0.9$) and is westward propagating. In the strongly unstable region the speed is $\omega/k_y = 1/2\, v_{di} = \overline{v_i(\rho_i/2L_p)}$ and in the weakly unstable high beta region the speed is $\omega/k_y = v_d i(x)$. These waves are in the 2 mHz-20 mHz (Pi 2 and Pc5) range and propagate westward with speeds of 5 to 10 km/s.

FIG. 5. Zeroth order perturbed parallel magnetic field, Q_L, as a function of position along the field line computed using the eigenfunction from fast MHD ballooning mode equation and the constant current field model.

FIG. 6. The IMF, MLT, and latitude dependence of (a) the flux tube volume, (b) the equitorial crossing point of the flux tube in the magnetotail, (c) the field line length and (d) the locus of footpoints in the magnetosphere as a function of latitude. The values are computed with Tsyg 96 for local times 2200 (blue curves) and 2400 (red curves), corresponding to auroral field lines. The solid curves have a northward IMF and the dashed curves have a southward IMF. The conditions chosen for the model were $P_{\rm dyn} = 3.0nPa$, $D_{\rm st} = -50nT$, $B_y^{\rm IMF} = 0.0$, and $B_z^{\rm IMF} = \pm 10.0nT$.

FIG. 7. In all panels the energies are computed along the equitorial plane, the wave function is taken to be $X(s) = (1R_E{\cdot}1\, nt)\exp(-s^2/\sigma^2)$ where $\sigma = 1.5R_E$. Formulas for the energies come from Horton *et al.* (1999). Panel (a) shows the energy required to bend the magnetic field. Panel (b) gives the kinetic energy in the flux tube divided by the growth rate squared. In panel (c) we give two versions of the energy required to compress the plasma (The blue line was computed from the kinetic formula, the red line is from the MHD formula with $\gamma = 5/3$). In panel (d) we have the unstable pressure gradient driven energy, in which the pressure gradient was increased by a factor of 6.0 over the Tsyg 96 value to make the system unstable. Panel (e) shows the sum of panels (a,c,d) which gives the total potential energy. Panel (f) gives the growth rate computed by dividing the potential energy by the kinetic.

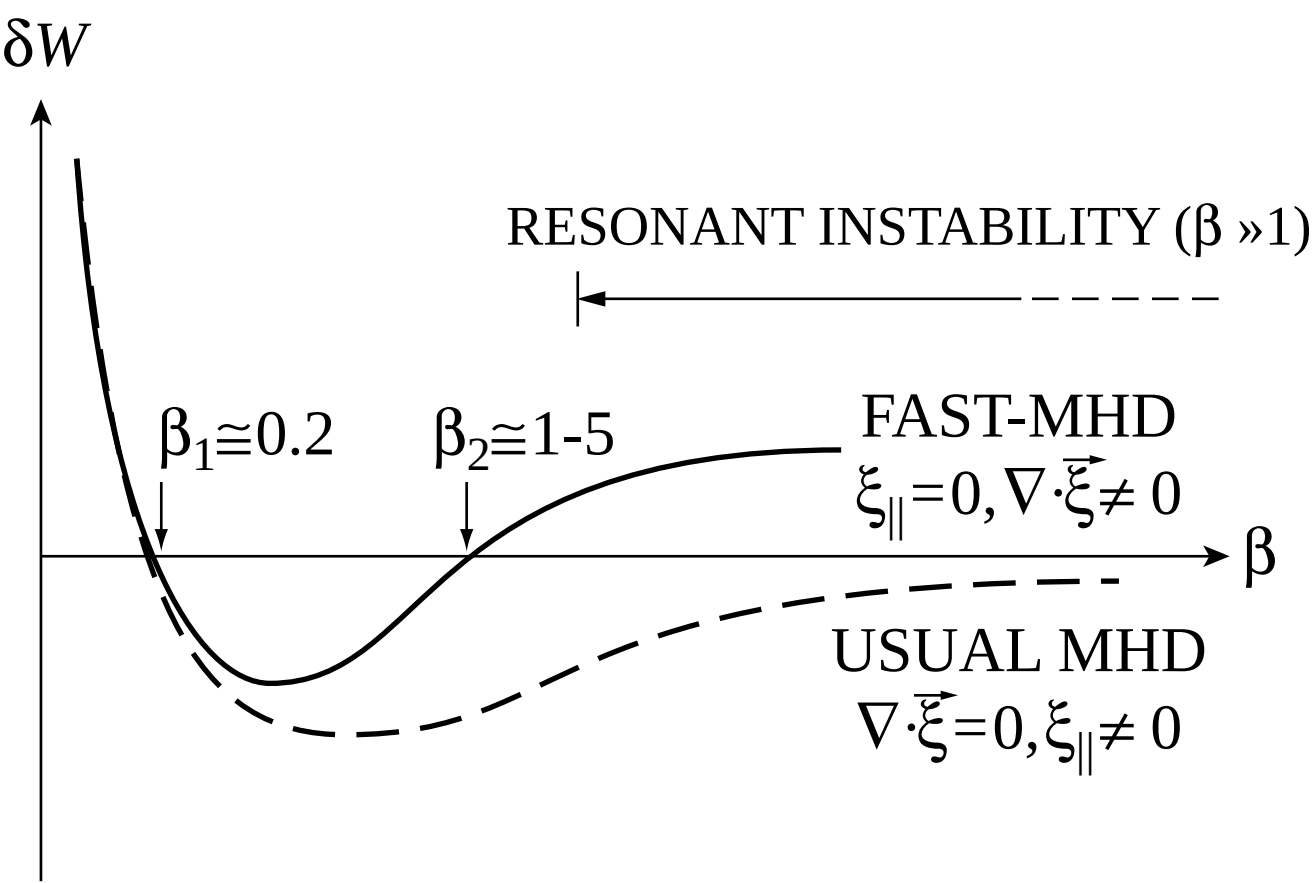
δW
RESONANT INSTABILITY (β »1)
β1≅0.2
β2≅1-5
FAST-MHD
ξ||=0, ∇·ξ⃗≠ 0
β
USUAL MHD
∇·ξ⃗=0, ξ||≠ 0

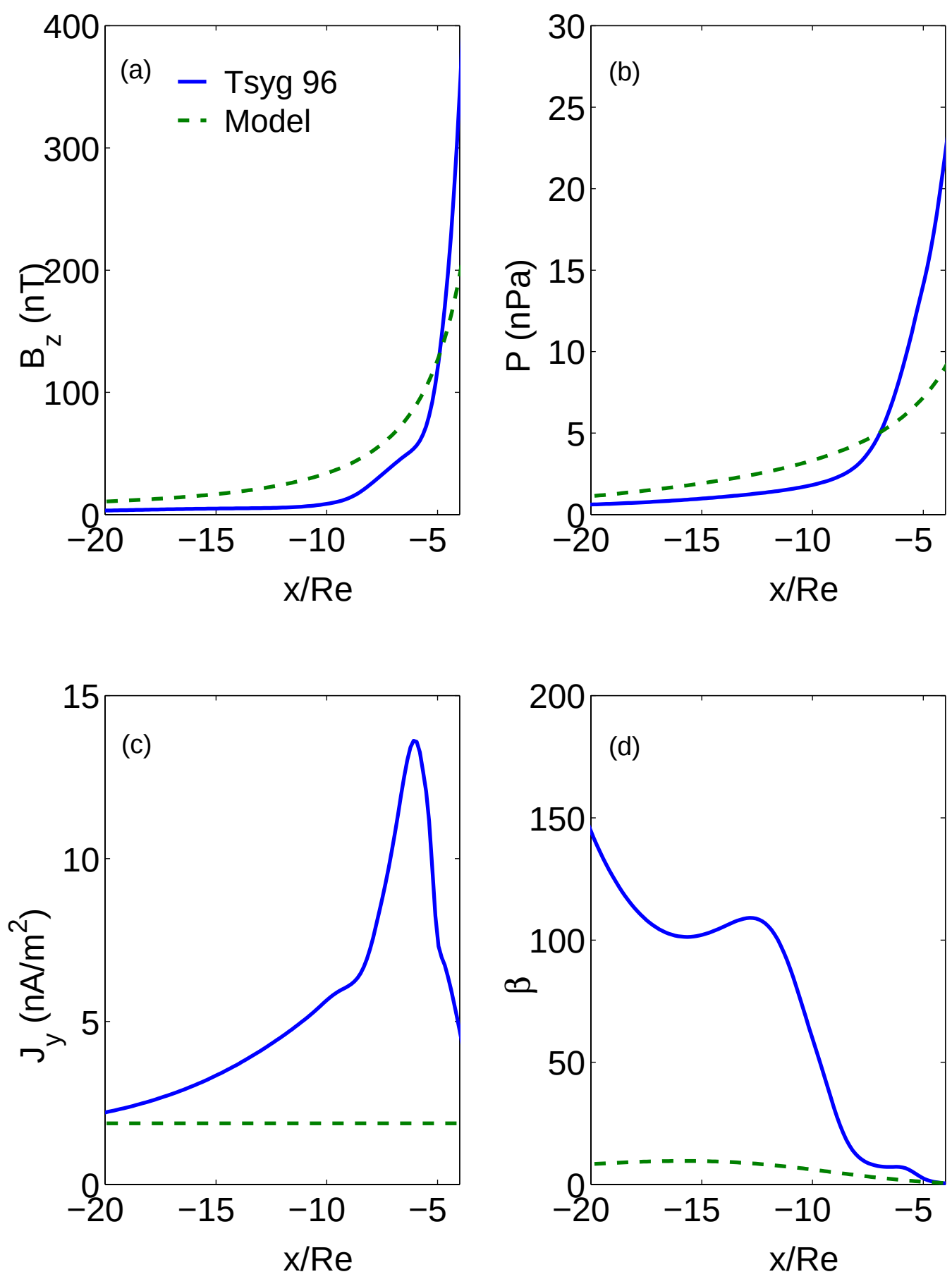
(a)
Tsyg 96
Model
400
300
200
100
0
B_z (nT)
−20
−15
−10
−5
x/Re
(b)
30
25
20
15
10
5
0
P (nPa)
−20
−15
−10
−5
x/Re
(c)
15
10
5
0
J_y (nA/m^2)
−20
−15
−10
−5
x/Re
(d)
200
150
100
50
0
β
−20
−15
−10
−5
x/Re

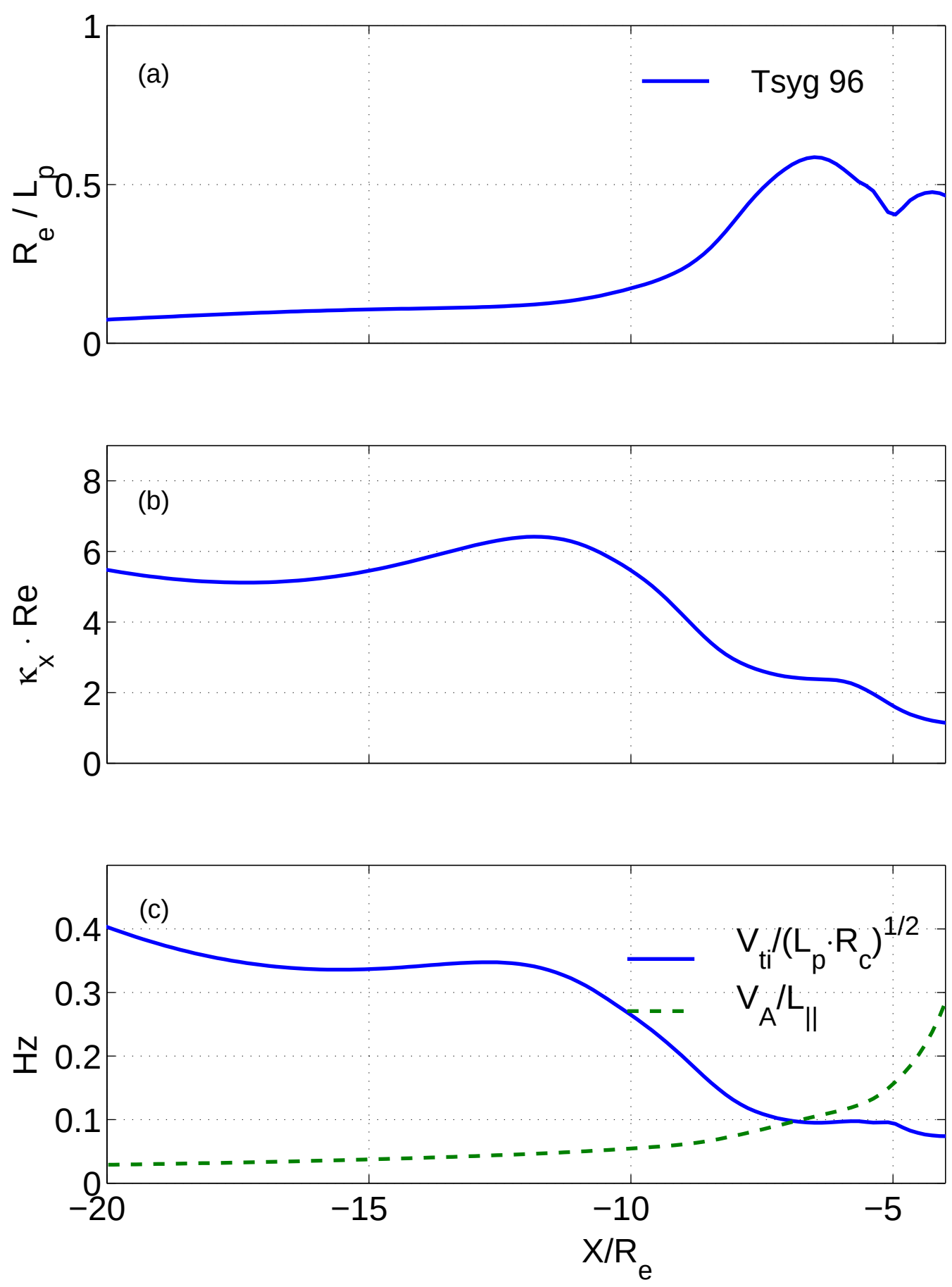
(a)
Tsyg 96
R_e / L_p
1
0.5
0
(b)
$\kappa_x \cdot Re$
8
6
4
2
0
(c)
$V_{ti}/(L_p \cdot R_c)^{1/2}$
$V_A/L_{||}$
Hz
0.4
0.3
0.2
0.1
0
−20
−15
−10
−5
X/R_e

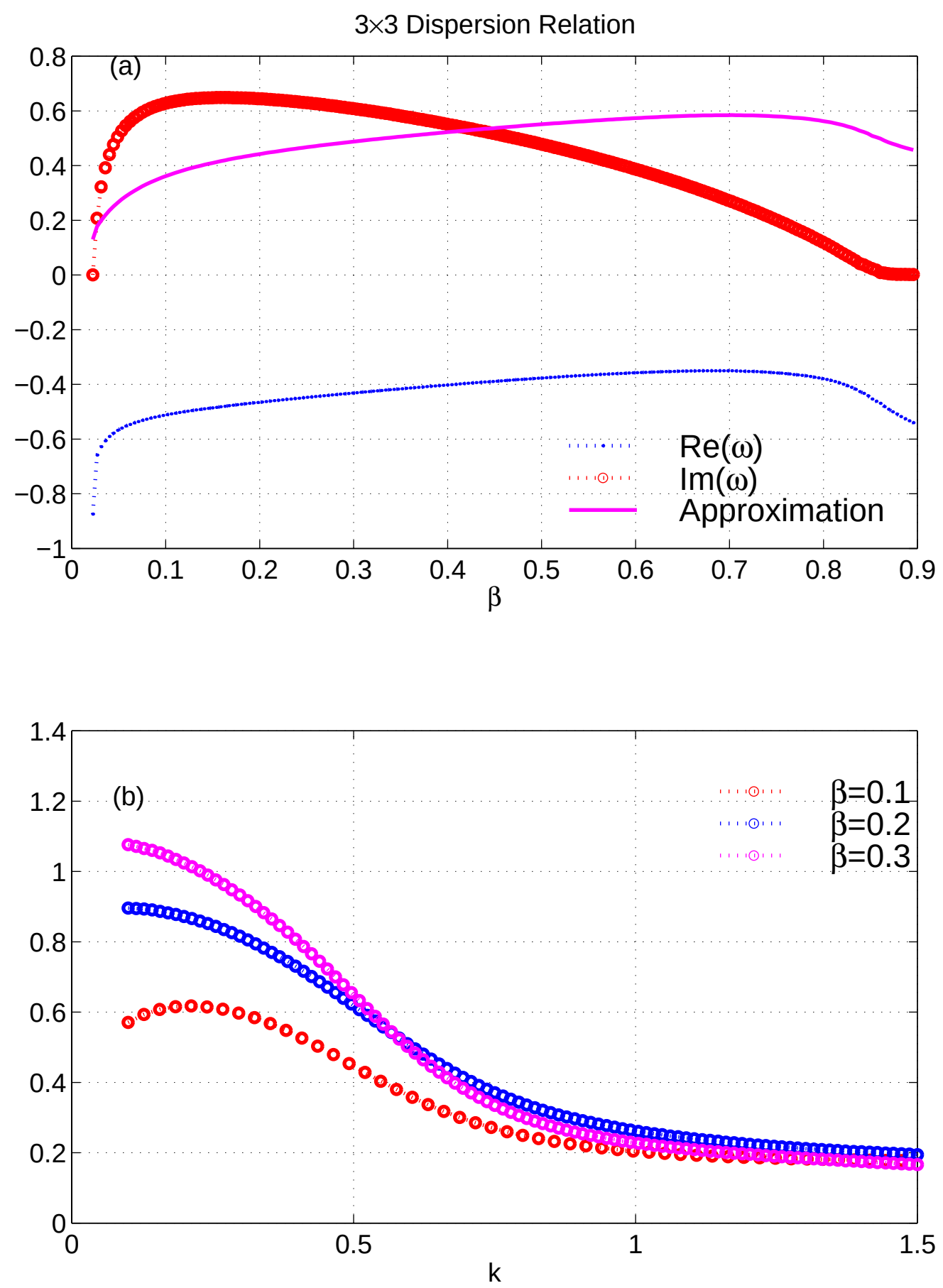
3×3 Dispersion Relation
(a)
0.8
0.6
0.4
0.2
0
−0.2
−0.4
−0.6
−0.8
−1
0
0.1
0.2
0.3
0.4
0.5
0.6
0.7
0.8
0.9
β
Re(ω)
Im(ω)
Approximation
(b)
1.4
1.2
1
0.8
0.6
0.4
0.2
0
0
0.5
1
1.5
k
β=0.1
β=0.2
β=0.3

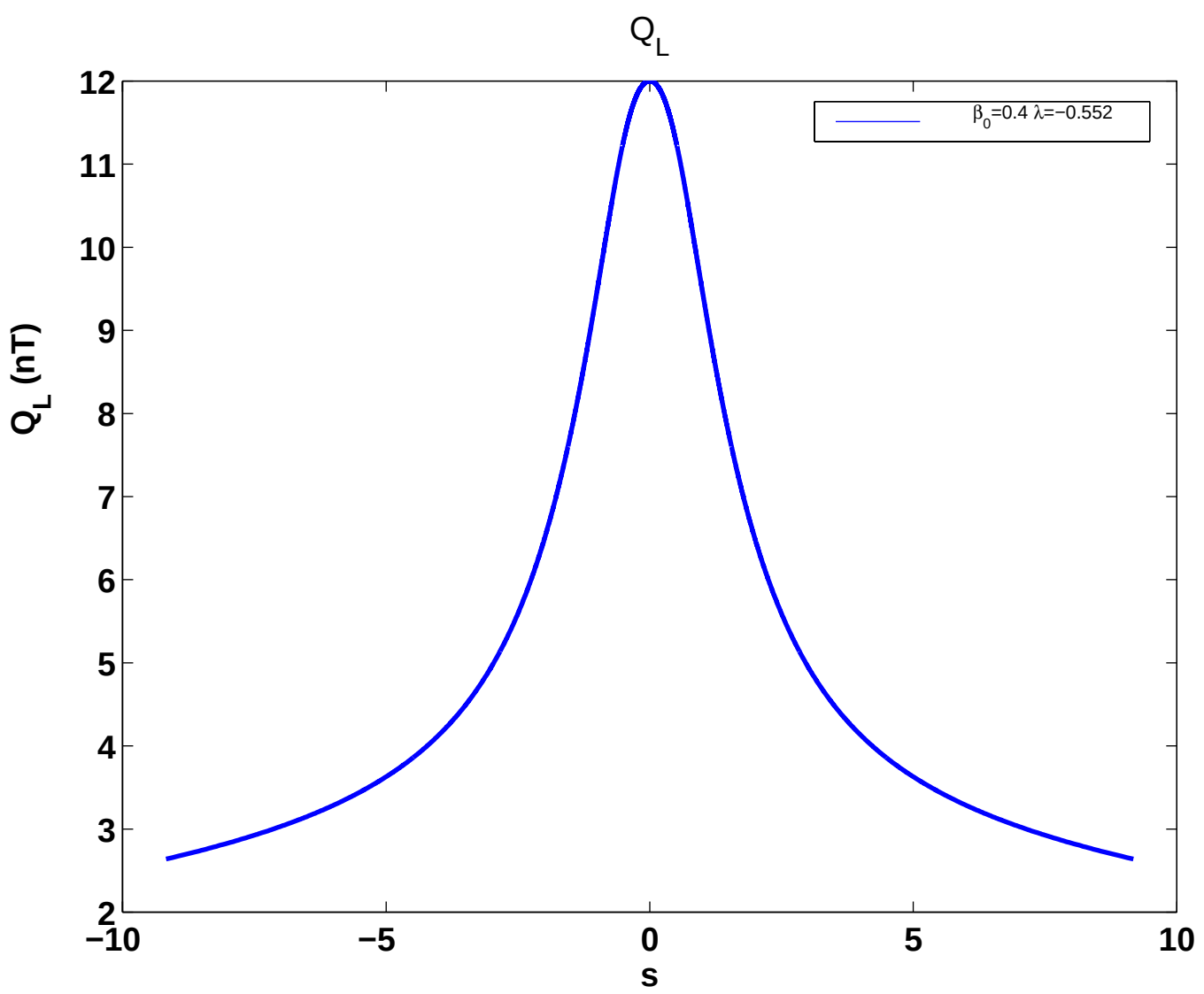
Q_L
β_0=0.4 λ=−0.552
Q_L (nT)
12
11
10
9
8
7
6
5
4
3
2
−10
−5
0
5
10
s

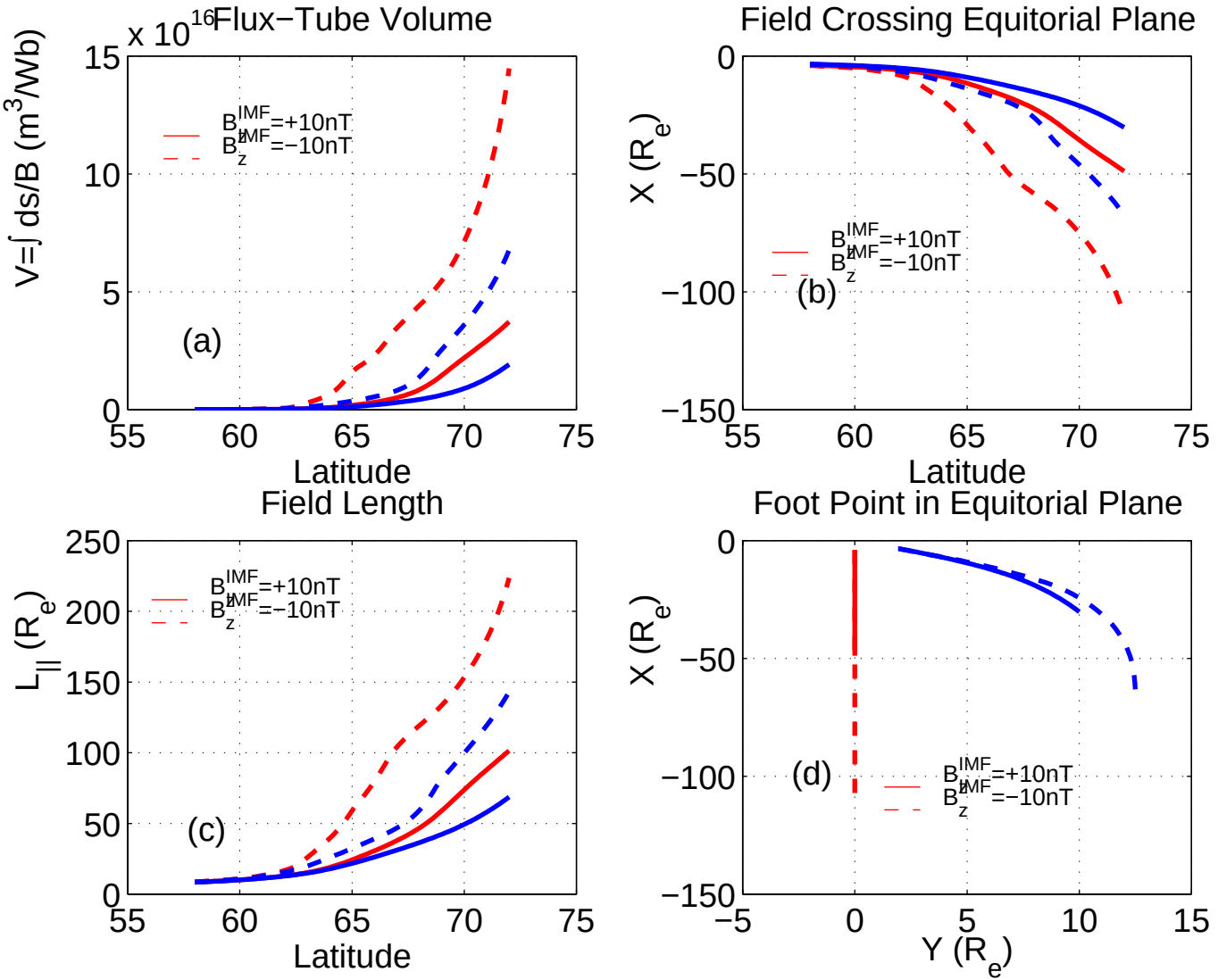
Flux−Tube Volume
x 10^16
V=∫ ds/B (m^3/Wb)
B_z^IMF=+10nT
B_z^IMF=−10nT
(a)
Latitude
Field Crossing Equitorial Plane
X (R_e)
(b)
Latitude
Field Length
L_|| (R_e)
(c)
Latitude
Foot Point in Equitorial Plane
X (R_e)
(d)
Y (R_e)

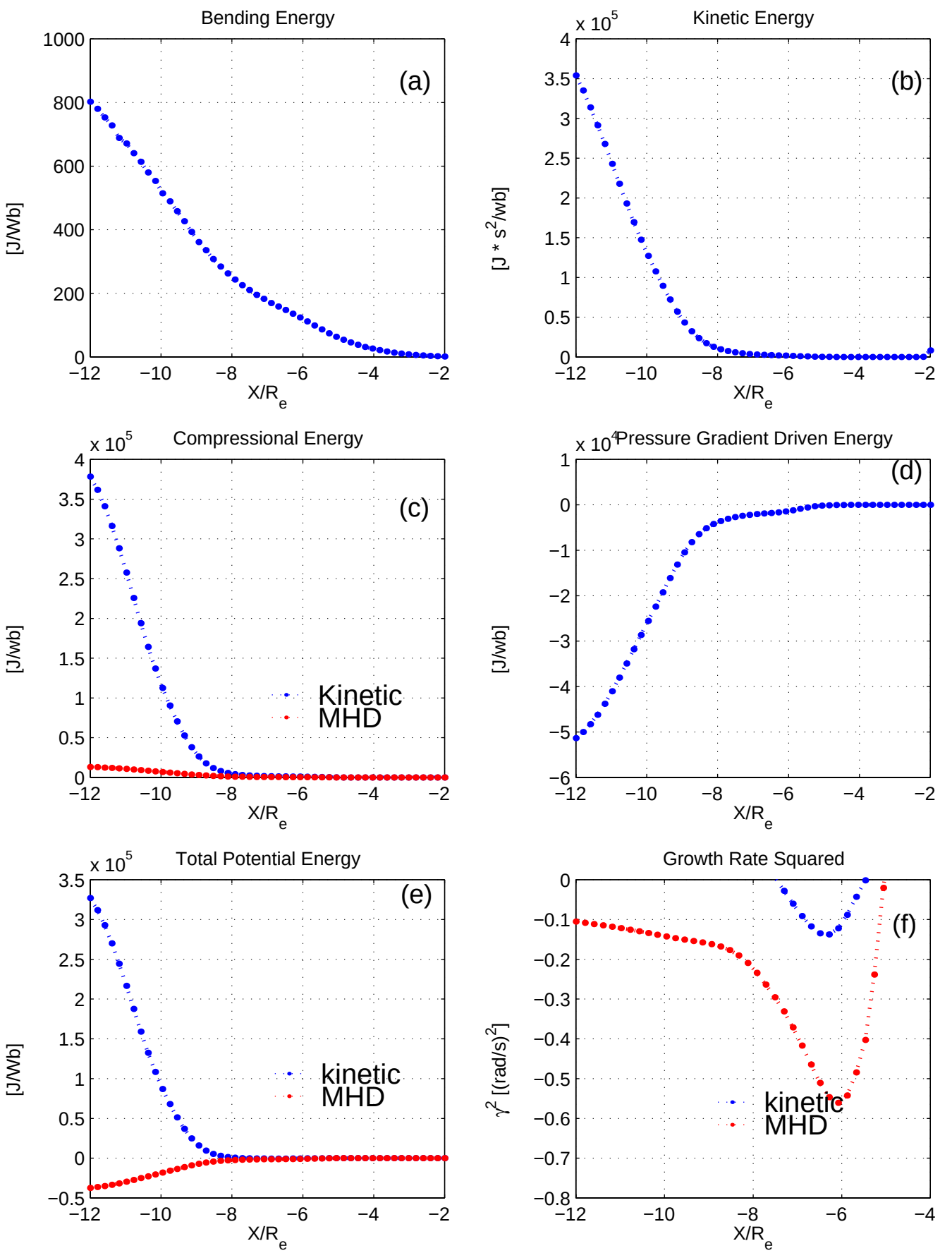
Bending Energy
(a)
[J/Wb]
X/R_e
Kinetic Energy
x 10^5
(b)
[J * s^2/wb]
X/R_e
Compressional Energy
x 10^5
(c)
Kinetic
MHD
[J/wb]
X/R_e
Pressure Gradient Driven Energy
x 10^4
(d)
[J/wb]
X/R_e
Total Potential Energy
x 10^5
(e)
kinetic
MHD
[J/Wb]
X/R_e
Growth Rate Squared
(f)
kinetic
MHD
γ^2 [(rad/s)^2]
X/R_e